JOURNAL OF GEOPHYSICAL RESEARCH, VOL. 102, NO. B9, PAGES 20,873–20,896, SEPTEMBER 10, 1997

Deep seismic structure and tectonics of northern Alaska: Crustal-scale duplexing with deformation extending into the upper mantle

Gary S. Fuis, Janice M. Murphy, William J. Lutter,[1]
Thomas E. Moore, and Kenneth J. Bird
U.S. Geological Survey, Menlo Park, California

Nikolas I. Christensen
Department of Geosciences, Purdue University, West Lafayette, Indiana

Abstract. Seismic reflection and refraction and laboratory velocity data collected along a transect of northern Alaska (including the east edge of the Koyukuk basin, the Brooks Range, and the North Slope) yield a composite picture of the crustal and upper mantle structure of this Mesozoic and Cenozoic compressional orogen. The following observations are made: (1) Northern Alaska is underlain by nested tectonic wedges, most with northward vergence (i.e., with their tips pointed north). (2) High reflectivity throughout the crust above a basal decollement, which deepens southward from about 10 km depth beneath the northern front of the Brooks Range to about 30 km depth beneath the southern Brooks Range, is interpreted as structural complexity due to the presence of these tectonic wedges, or duplexes. (3) Low reflectivity throughout the crust below the decollement is interpreted as minimal deformation, which appears to involve chiefly bending of a relatively rigid plate consisting of the parautochthonous North Slope crust and a 10- to 15-km-thick section of mantle material. (4) This plate is interpreted as a southward verging tectonic wedge, with its tip in the lower crust or at the Moho beneath the southern Brooks Range. In this interpretation the middle and upper crust, or all of the crust, is detached in the southern Brooks Range by the tectonic wedge, or indentor: as a result, crust is uplifted and deformed above the wedge, and mantle is depressed and underthrust beneath this wedge. (5) Underthrusting has juxtaposed mantle of two different origins (and seismic velocities), giving rise to a prominent sub-Moho reflector.

Introduction

The Brooks Range, northern Alaska, is a compressional orogen that is an extension of the western North American Cordillera [*Oldow et al.*, 1989; *Grantz et al.*, 1991]. Formation of the Brooks Range began in the Late Jurassic and Early Cretaceous, as the passive margin of North America was subducted and telescoped beneath an intraoceanic arc; this subduction zone dipped southward in present coordinates. Following the initial collision, an ocean basin underlying the present Arctic Ocean opened north of the orogen in mid- to Late Cretaceous time; the current passive margin along northern Alaska was rifted from northern Canada by rotation [*Grantz and May*, 1983; *Plafker and Berg*, 1994] and/or by left-slip faulting [*Oldow et al.*, 1989]. The Brooks Range differs from the Cordillera farther south in the excessive shortening postulated for it, more than 500 km [*Mayfield et al.*, 1983; *Oldow et al.*, 1987] versus a few hundred kilometers for other parts of the Cordillera [*Oldow et al.*, 1989].

Several models for the structure and evolution of the Brooks Range have been advanced. Using surface mapping and available industry reflection data, *Mull et al.* [1987] and *Oldow et al.* [1987] constructed cross sections of the Brooks Range orogen showing crustal-scale duplexing on chiefly north vergent thrust faults. The cross section of *Oldow et al.* [1987] was further constrained by balancing of the cross-sectional areas of the various geologic units. Using surface mapping, seismic refraction data, and gravity data, *Grantz et al.* [1991] produced a cross section showing upper crustal duplexing on north vergent thrust faults but lower crustal duplexing on south vergent (north dipping) thrust faults. Using surface mapping and petrofabric data, *Miller and Hudson* [1991] emphasized the role of extensional collapse in the shaping of the orogen.

In 1990, in order to test these models of the Brooks Range structure and evolution, we conducted a seismic reflection and refraction survey through the region and collected a suite of rock samples for laboratory velocity analysis. This northern Alaskan survey was also undertaken as the final leg of the Trans-Alaska Crustal Transect (TACT), a multidisciplinary investigation of the lithosphere of Alaska from Pacific to Arctic margins. For a description of the seismic data collected in northern Alaska and previous interpretations of that data, see *Murphy et al.* [1993], *Levander et al.* [1994], and *Fuis et al.* [1995].

The results and interpretations summarized by *Fuis et al.* [1995] were based on a seismic velocity model obtained by

[1]Now at Department of Geology and Geophysics, University of Wisconsin-Madison.

Paper number 96JB03959.
0148-0227/97/96JB-03959$09.00

inverse modeling of both first- and second-arrival travel times and on common midpoint (CMP) images of near-vertical-incidence reflections. In this paper these results are largely substantiated and detailed using forward modeling techniques. In addition, new results for the northern Brooks Range and North Slope are presented, as well as new results for the Moho and a sub-Moho reflector. This study also integrates laboratory rock velocity results and data from oil wells on the North Slope into the final model.

Geologic Setting and Definition of the Problems

The Brooks Range is a west trending, north vergent orogenic belt that formed along a part of the North American continental margin that faced south (in present coordinates) in the Late Jurassic and Early Cretaceous. Widespread high-pressure metamorphism in the continental rocks of the southern Brooks Range, the presence of ophiolites at the highest structural levels, and the absence of a Mesozoic magmatic belt suggest the subduction was southward, beneath an intraoceanic volcanic arc [*Roeder and Mull*, 1978; *Moore et al.*, 1994, this issue]. Retrograde metamorphism and younger normal faults indicate that contraction was followed by extension in the mid-Cretaceous [*Gottschalk and Oldow*, 1988; *Miller and Hudson*, 1991]. The Koyukuk basin, south of the Brooks Range, is underlain by a Jurassic(?) and Early Cretaceous island arc terrane that overrode the Arctic Alaska terrane during subduction. A foreland basin of Albian and younger age (Coleville basin) is present north of the Brooks Range, beneath the North Slope.

The northern continental margin of Alaska is a passive margin formed by the opening of the Canada basin (Plate 1, inset). This opening occurred in the mid- to Late Cretaceous by counterclockwise rotation of the Arctic Alaska terrane away from Canadian North America, about a pole near the present Mackensie River delta (300–400 km east of the U.S./Canada border, Plate 1 [*Grantz and May*, 1983; *Plafker and Berg*, 1994]). Alternatively, *Oldow et al.* [1989] have proposed that the passive margin was created by left-slip faulting along the eastern boundary of the Brooks Range accompanied by rifting along the current passive margin. Uplift and contraction have continued into the Cenozoic in the northeastern Brooks Range and produced the northeastern salient of the Brooks Range and the Mount Doonerak antiform in the interior of the range [*Wallace and Hanks*, 1990; *O'Sullivan et al.*, 1993, 1997].

Northern Alaska consists of the continental Arctic Alaska terrane and the oceanic Angayucham terrane. The Arctic Alaska terrane has been subdivided into a number of subterranes, including the sedimentary North Slope, Delong Mountains, and Endicott Mountains subterranes (abbreviated NSS, DMS, and EMS, respectively), and the predominantly metasedimentary Hammond, Coldfoot, and Slate Creek subterranes (Plate 1) [*Moore et al.*, 1994; this issue]. In the subsurface of the North Slope the NSS has a basement of deformed continental rocks (Franklinian sequence: Proterozoic through Middle Devonian), overlain in turn by stable shelf and rift-filling sedimentary rocks (Ellesmerian sequence: Mississippian through Lower Cretaceous, including carbonate rocks of the Lisburne Group, of Mississippian and Pennsylvanian age) and by foredeep deposits shed from the Brooks Range (Brookian sequence: Lower Cretaceous through Cenozoic). Franklinian and Ellesmerian rocks of this subterrane are exposed in the northeastern Brooks Range, east of the transect, and in the Doonerak window in the north central Brooks Range, west of the transect (Plate 1). The DMS and EMS contain rocks that are correlative with the NSS Ellesmerian rocks; in addition, both contain Upper Devonian sedimentary rocks. The DMS and EMS structurally overlie the NSS and may locally underlie the Brookian sequence along a backthrust on the north side of the Brooks Range. The Hammond subterrane (upper Proterozoic? to Upper Devonian greenschist-facies rocks) lies structurally below the EMS along its northern margin and above the Coldfoot subterrane on the south (Proterozoic to middle Paleozoic blueschist-facies rocks overprinted by greenschist facies), although the structural position of this subterrane on a regional basis is uncertain [cf. *Oldow et al.*, 1987]. The Slate Creek subterrane (middle to late Paleozoic) consists predominantly of phyllonite and melange that compose a belt along the south margin of the Brooks Range [*Moore et al.*, 1994, this issue]. The phyllonite was formed by normal faulting under ductile conditions in the mid-Cretaceous.

The ophiolitic Angayucham terrane (Devonian to Lower Jurassic) separates the Arctic-Alaska terrane from the island arc Koyukuk terrane in the Koyukuk basin, south of the Brooks Range. Along the transect, the Angayucham terrane consists of a tectonic assemblage of oceanic basalts and chert of late Paleozoic and early Mesozoic age.

Along the southeast side of the Koyukuk basin, several terranes are lithologically similar to terranes and subterranes in the Brooks Range as follows: Ruby terrane (similar to the Coldfoot terrane), Prospect Creek terrane (similar to the Slate Creek subterrane), and Tozitna terrane (similar to the Angayucham terrane). These terranes may be equivalents of the terranes in the Brooks Range that have moved southward during extension in the mid-Cretaceous [*Miller and Hudson*, 1991]. On the other hand, they may represent an eastern part of the Brooks Range that moved southwestward by right-lateral strike-slip motion in the Late Cretaceous [*Moore et al.*, 1994]. Finally, they may have achieved their current positions during oroclinal bending of northern Alaska [*Plafker and Berg*, 1994].

Geological cross sections along our transect by *Mull et al.* [1987], *Oldow et al.* [1987], and *Grantz et al.* [1991] all agree that (1) the EMS is a lens-shaped body, about 5 km thick, that was emplaced on a decollement above the NSS; (2) the Doonerak antiform is a crustal-scale duplex that exposes Franklinian and Ellesmerian rocks of the NSS; and (3) mid-Cretaceous (Brookian) foredeep deposits extend southward in varied thickness beneath the DMS and EMS. These cross sections differ principally in their portrayal of structural relationships in the southern Brooks Range; *Grantz et al.* [1991] were alone in suggesting north dipping structures in the middle and lower crust in the southern Brooks Range. A cross section by *Fuis et al.* [1995, Figure 5], elaborated upon in this paper, substantiates points 1 and 2 but not point 3 above. In addition, the transect data indicate north dipping structures in the middle crust of the southern Brooks Range possibly similar to those postulated by *Grantz et al.* [1991].

Data Acquisition

A 700-channel seismograph system was used to record 65 shots at 44 separate shotpoints (Plate 1) [*Murphy et al.*, 1993].

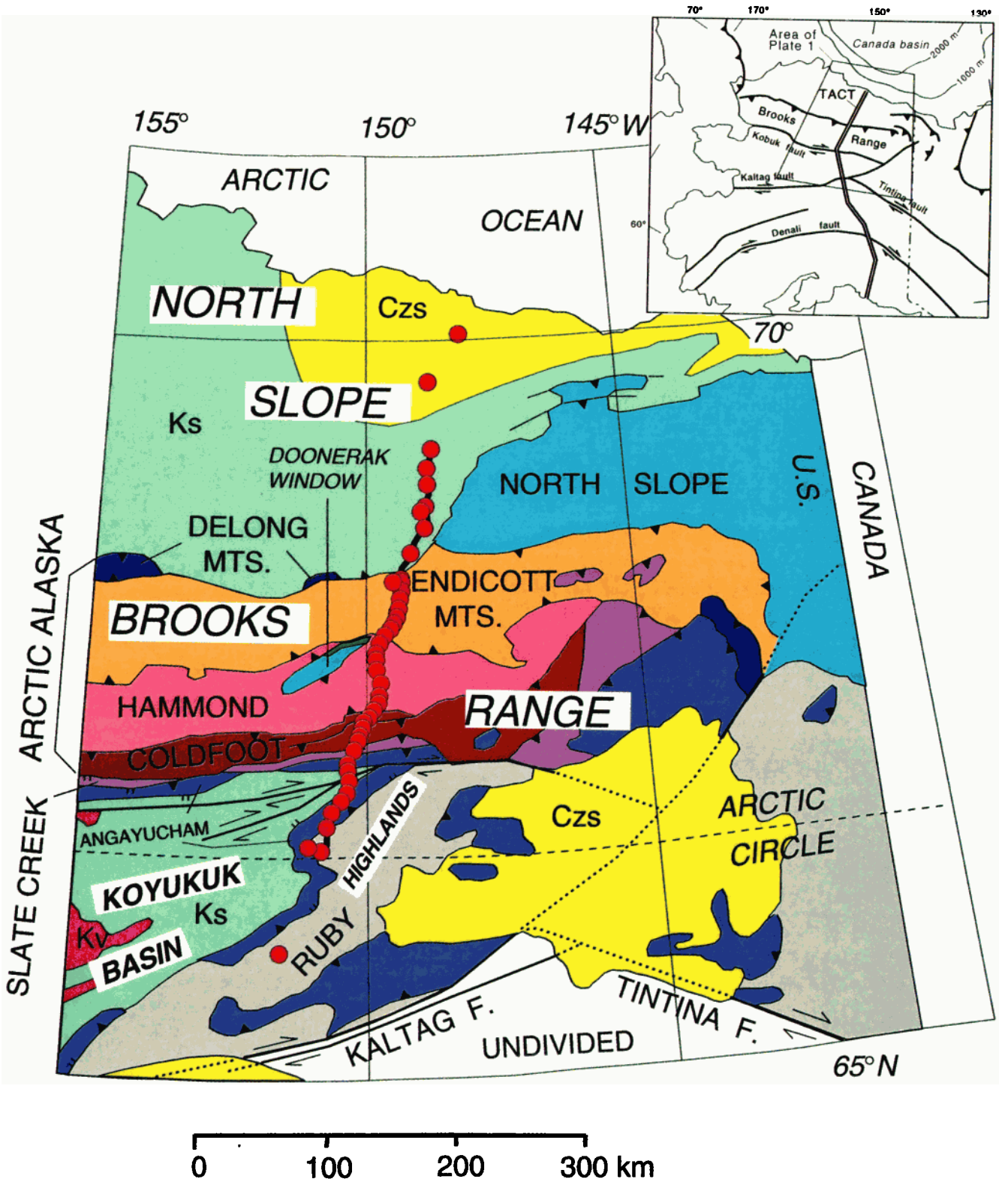

Plate 1. Terrane map of northern Alaska showing shot points (red dots) of 1990 seismic experiment. Terrane map was modified from *Grantz et al.* [1991]. Terrane and subterrane names appear in nonitalicized print: Arctic Alaska terrane comprises Brooks Range and North Slope and is subdivided, from north to south, into sedimentary North Slope, Delong Mountains, and Endicott Mountains subterranes and metasedimentary-metavolcanic Hammond, Coldfoot, and Slate Creek subterranes. Ophiolitic Angayucham terrane separates Arctic Alaska terrane from island arc Koyukuk terrane to the south. Ks, Cretaceous sedimentary rocks; Kv, Cretaceous volcanic rocks; Czs, Cenozoic sedimentary rocks. See Plate 3 for combined "explanation for map (Plate 1) and cross section (Plate 3)" for description of geologic units and symbols.

Table 1. Zones of Reflections in the Brooks Range

Zone	Range (Model Coordinates), km	Depth, km	Description of Reflections
A	240 to 295	2 to 9	strong; parallel to echelon; subhorizontal; gently arched near the Doonerak antiformal axis (240 km)
B	200 to 310	7 to 30	strong; parallel to echelon; linear; south dipping
C	140 to 240	2 to 17	moderate to weak; subhorizontal to gently south or north dipping
D	170 to 270	5 to 27	strong; curved to ramp-and-flat shaped; moderately south dipping on the ramps
E	120 to 190	6 to 23	moderate to weak; gently north dipping
F	south of 110 to north of 300	30 to 60 or deeper	diffuse vertical incidence reflections; zone is parallel to and includes the Moho (a wide-angle reflector) near its base; bifurcates into zones F1 and F2 near 275 km; F1 contains vertical incidence reflections parallel to Moho; F2 contains gently north dipping vertical incidence reflections within the mantle [see also *Wissinger et al.*, this issue]; wide-angle reflections within F2 appear to be subhorizontal
N (defined in this study)	295 to north of 400	2 to 11	strong to weak wide-angle reflections; synformal from 295 to 340 km; gently undulating from 340 to 400; south limb of synform merges with zone A; north limb of synform merges with zone B

Based on both vertical incidence and wide-angle reflection images, reflections can be grouped into seven zones, A–F and N (Plate 2) [*Fuis et al.*, 1995].

All seismographs recorded vertical component motion only. The instruments were deployed five times in abutting and overlapping arrays, ranging in length from 70 to 120 km, producing a profile totaling 315 km in length. Instrument spacing nominally was 100 m. Both small shots (45–275 kg) within arrays and large shots (680–1800 kg) off the ends of the arrays were fired to produce a vertical incidence to wide-angle refraction-reflection data set. Shots were fired repeatedly at five shot points to produce continuous coverage from 0- to over 200-km range at 100-m instrument spacing. Shallow (3- to 6-m-deep) lakes were used for most of the largest shots. In-line shot spacing averaged 8 km, and signal-to-noise ratios were excellent for most shots.

Previous Studies

Prior to this study, the seismic data were processed in several ways to produce different but complementary images of the Brooks Range. These images included (1) near-vertical-incidence reflection sections, both low-fold and single-fold sections, (2) a wide-angle reflection section, and (3) an inversion-derived seismic velocity model. These sections extended from the highlands southeast of the Koyukuk basin (also known as the Kokrine-Hodzana highlands [*Wahrhaftig*, 1965]) to the northern range front and are shown and described by *Levander et al.* [1994] and *Fuis et al.* [1995]. Zones of reflections described by *Fuis et al.* [1995] are described in Table 1, and these zones are shown on the new velocity model (Plate 2). The interpretations of *Fuis et al.* [1995] are basically supported in this study with the exception of some details near the northern range front (see Interpretation section, below).

Results of This Study

This study extends the wide-angle reflection section (item 2 of Previous Studies section) well onto the North Slope (Plate 2) and incorporates oil-well data from the North Slope (Plate 2 and Figure 1) into the model. In addition, the Moho and a prominent sub-Moho reflection are studied in detail, and a forward seismic velocity model of both the Brooks Range and North Slope is presented (Plate 2). The purposes of the forward modeling include both checking travel time picks and refining the inversion-derived velocity model (item 3 of Previous Studies section). The reader is referred to *Wissinger et al.* [this issue] for a new version of the near-vertical-incidence image (item 1 of Previous Studies section).

Wide-Angle Reflection Data

The wide-angle-reflection section presented by *Fuis et al.* [1995, Figure 3] was constructed independently of the near-vertical-incidence reflection sections using a very simple technique [*Fuis et al.*, 1992]. For a given wide-angle reflection, one examines all pairs of shot gathers from which reciprocal times for that reflection can be determined. For illustration, at least five wide-angle reflections can be traced between shot points (SPs) 133 and 174 (model coordinates 204 and 223 km) (Plate 2), located in the central, highly reflective part of the Brooks Range (Figures 2a and 2b). Reciprocal arrival times are marked with small vertical travel time error bars at each shot point. Reciprocal arrival times at other shot points are also indicated by error bars. Such plots of reciprocal times allow one to project wide-angle reflections to zero range, or vertical incidence, where they can be identified with the appropriate vertical incidence reflections. By connecting such independently determined vertical incidence times on a plot of shot point distance versus time, one can trace these projected wide-angle reflections from shot point to shot point to determine geometrical interrelationships and interconnections [*Fuis et al.*, 1995, Figure 3]. Many such projected wide-angle reflections can be traced for distances of up to 30 km, and important structural details within zones of vertical incidence reflections can be observed. After migration, these wide-angle reflections can be plotted in a depth section (Plate 2).

In this study, wide-angle reflections from six shot points in the northern Brooks Range and on the North Slope (SPs 141–189; model ranges 295–396 km; Plate 2) were made more visible by reprocessing so that they could be reliably traced to vertical incidence and correlated from shot gather to shot gather. Elimination of surface waves was accomplished by band-pass filtering, and surface statics (differing by as much as 0.1 s from receiver to receiver in the region from SP141 to 150; model ranges 295 to 335 km) were largely eliminated by shifting seismograms to align along smoothed travel time curves (obtained by applying a running average to first-arrival travel

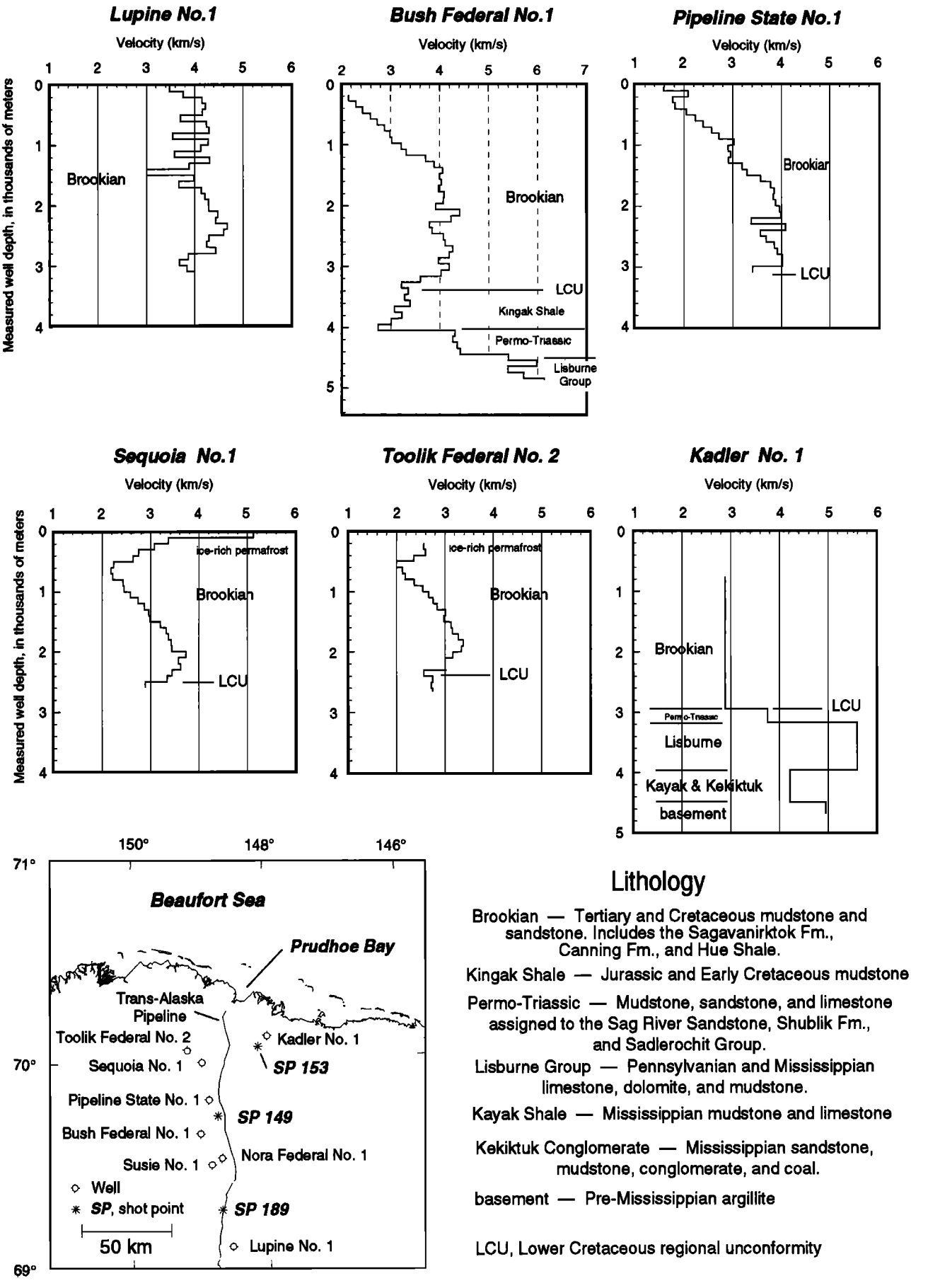

Figure 1. Oil well lithology and velocity data from North Slope.

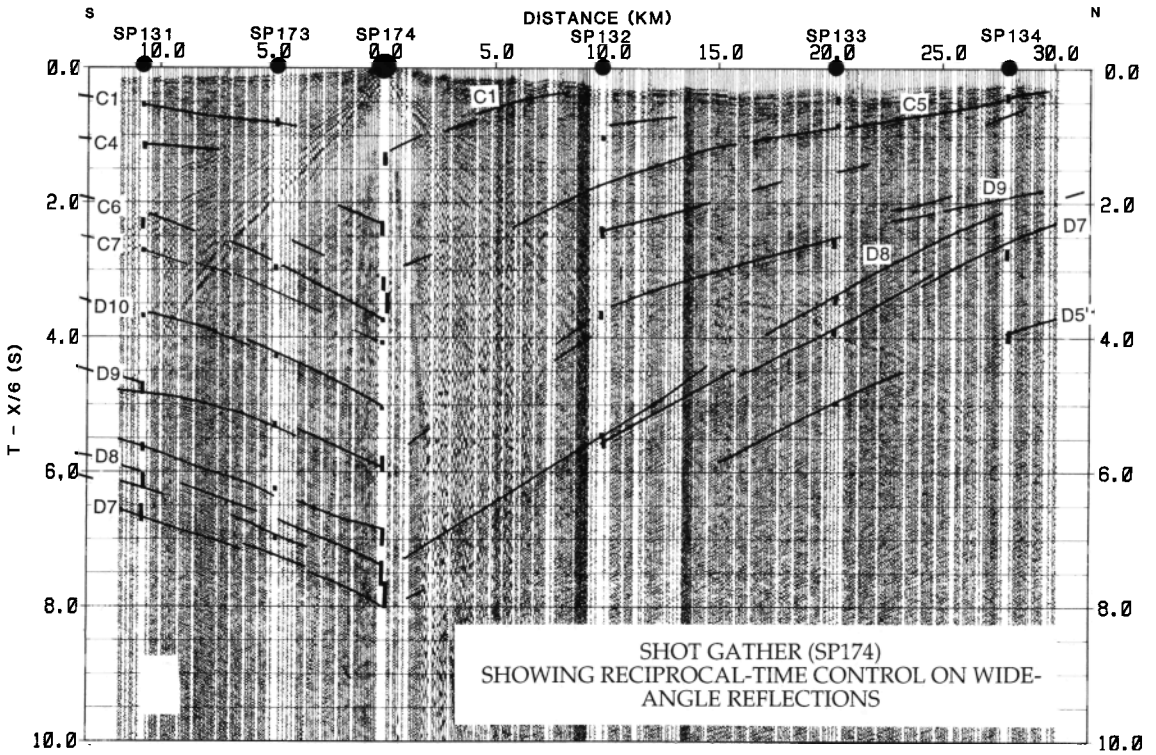

Figure 2a. Shot gather SP174 showing travel time curves for crustal phases and reciprocal time control (small travel time error bars below each shot point) on wide-angle reflections. Data were band-pass filtered, deconvolved, and automatic gain controlled (AGC). Reduced travel times ($T - x/6$ km/s) are shown. For identity of individual reflections (labeled C1, C4, etc.), see Plate 2. To map out reflections, this shot gather and others were used as follows: zero-range two-way travel times for each reflection were plotted below each shot point on travel time-distance plot and resulting dots were connected. Subsequent diagram was migrated and converted to depth-distance plot to obtain wide-angle reflections shown in Plate 2.

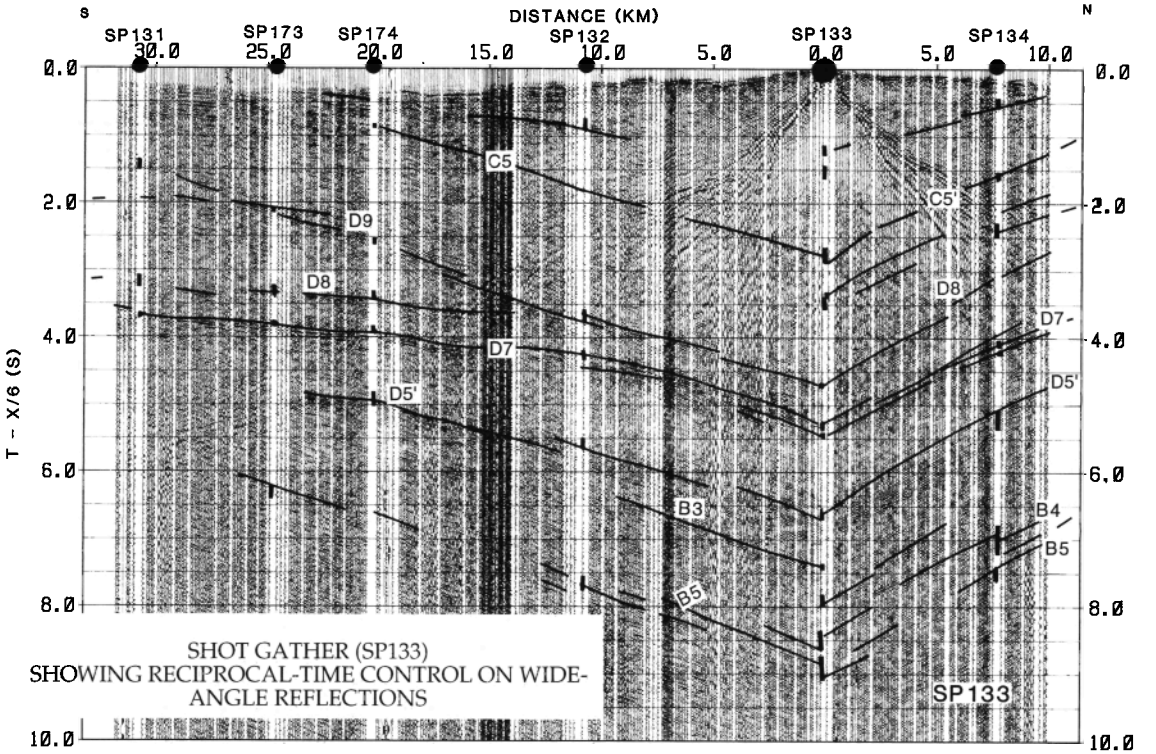

Figure 2b. Same as Figure 2a, except for SP133.

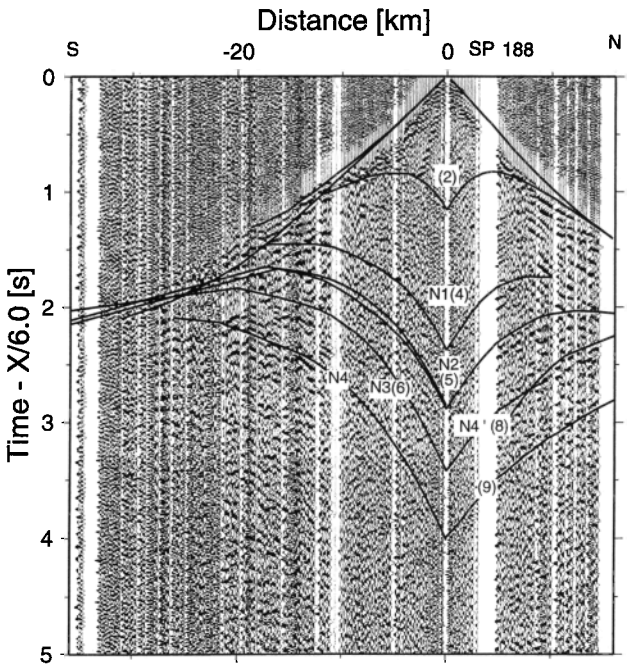

Figure 2c. SP188 displayed with reduced travel time. Data were band-pass filtered (minimum-phase filter) and automatic gain controlled. Travel time fluctuations in first arrivals were largely removed by applying elevation statics and by forcing first arrivals to fit smoothed travel time curves; this procedure enhanced reflections considerably (see text). For identity of individual reflections (labeled (2), N1(4), N2(5), etc.) see Plate 2; layer numbers (in parentheses) are given for some phases, including reflections from tops of layers and refractions from within layers. Arrival strength varies along most modeled branches. Note that applied minimum-phase filter delays reflections in data by about 40 ms compared to Figure 2d, where zero-phase filter is applied. Thus our calculated curves appear to fit the reflections better in Figure 2d than in Figure 2c.

times). In the reprocessed shot gathers, one can see numerous clear reflections (e.g., SP188; model coordinate 380 km; Figures 2c and 2d). The shot gathers were plotted with both reduced and unreduced travel time, and reflections were picked consistently on both gathers. (Some reflections were more easily correlated on one type of shot gather than the other; thus, both were useful. Note that in Figures 2a–2h, reflections are not traceable with the same sharpness and reliability along all parts of the hyperbolae in either type of plot. Note also that a few unmodeled reflections appear in the data; some of these are shown diagrammatically with unlabeled light-dashed lines in Plate 2.) For shot points 150 and 142 (model coordinates 335 and 315 km), oppositely asymmetric reflection hyperbolae are seen (Figures 2e, 2f, 2g, and 2h). These reflections indicate interfaces that form a broad synform-like structure at the northern range front (interfaces bounding layers 4 and 5; Plate 2). At least three south dipping interfaces are interpreted from the shot gathers for SP150, and at least two north dipping ones are seen from SP142.

On the North Slope, all labeled wide-angle reflections were ray traced (Plate 2; see description of forward modeling below). Within the Brooks Range, wide-angle reflections had been previously migrated and plotted on a distance-depth plot using the inversion-derived velocity model [*Fuis et al.*, 1995]. In this study, those reflections along or near the top of layer 6 were adjusted a bit in depth (a few tenths of a kilometer) by ray tracing; those along the top of layer 9, an arbitrary boundary along some of the strongest reflections in the midcrust, were checked by raytracing and found to be correctly placed (Plate 2).

To summarize the results of this study of wide-angle reflections (Plate 2), a large-scale (40 km wide) synform is seen at the northern range front. The north limb appears to be an extension of reflections of zone B (see Table 1). Farther north, the reflections define gently undulating layers (forming synforms and antiforms).

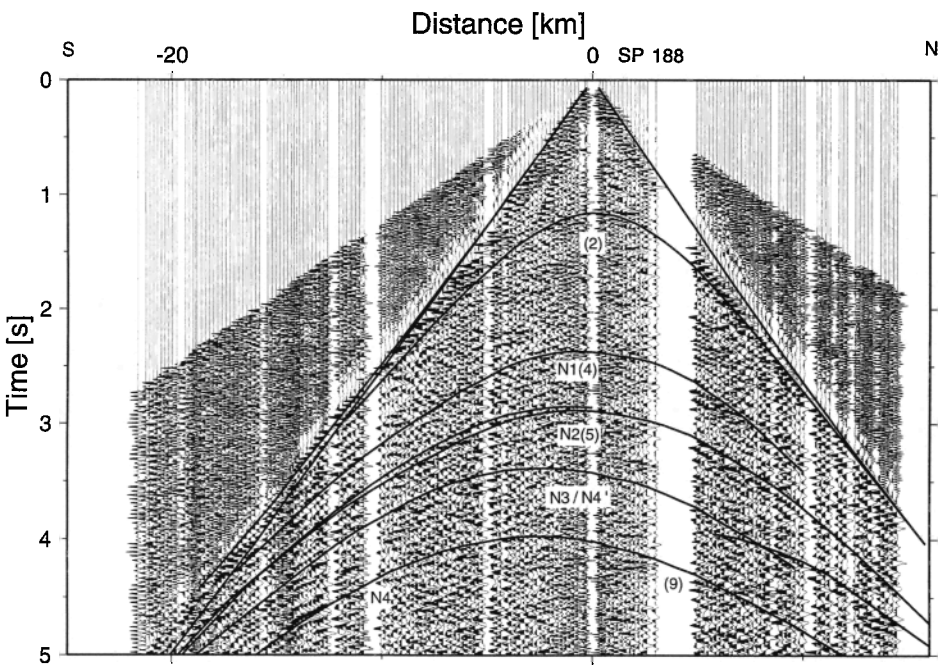

Figure 2d. SP188 displayed with unreduced travel time. Data were band-pass filtered (zero-phase filter) and automatic gain controlled.

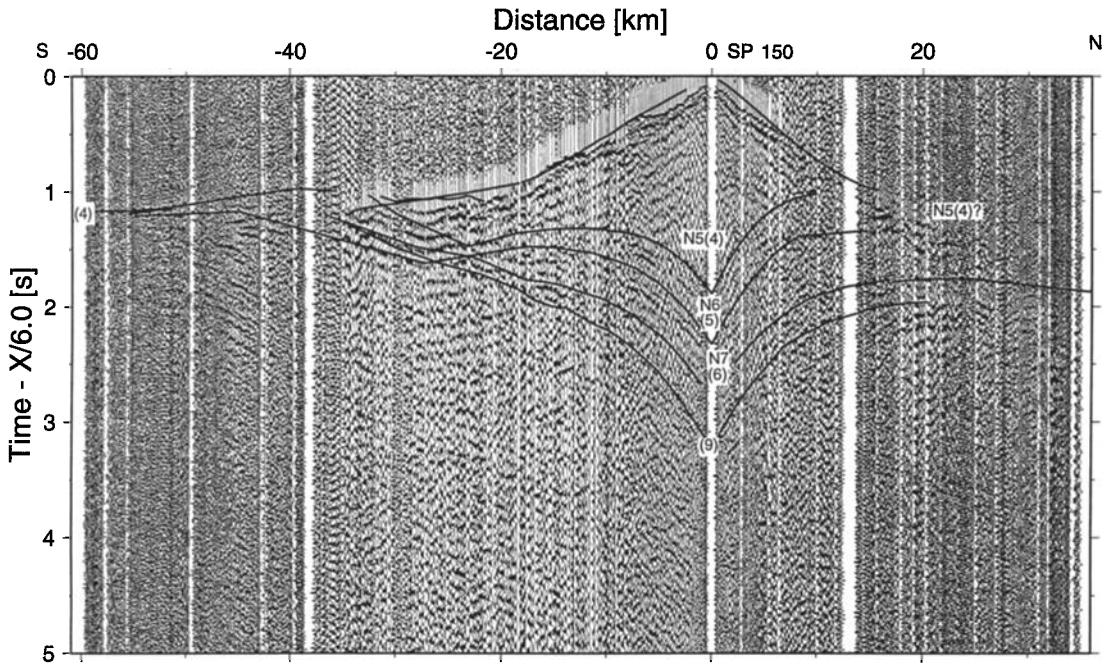

Figure 2e. SP150 displayed with reduced travel time. See caption for Figure 2c for further explanation. Asymmetry of reflections N5(4) and N6(5) indicate southward dip of reflectors.

Forward Velocity Model

The forward modeling method for determining crustal structure is discussed, for example, by *Blundell* [1984], *Meissner* [1986], and *Mooney* [1989]. Using the inverse model of *Fuis et al.* [1995] as a starting model (rms 0.06 s for first arrivals, 0.1–0.3 s for second arrivals), we iteratively modified the model using the interactive ray-tracing program MacRay [*Luetgert*, 1992], with the goal of matching first and second arrivals within 0.05 s, cusps (amplitude maxima) within 5 km, and branch terminations within 5 km. Mismatches as large as 0.2 s in travel time and 15 km for cusps and branch terminations are still present in places, however. The travel time rms, if calculated, would probably be approximately 0.10–0.15 s. An effort was made to calculate all phases predicted by the model for comparison with the data. Our model is, of course, not unique, given lateral velocity variation and the presence of low-velocity zones. Interface depths and velocities determined by both refractions and reflections (solid black lines and black numbers

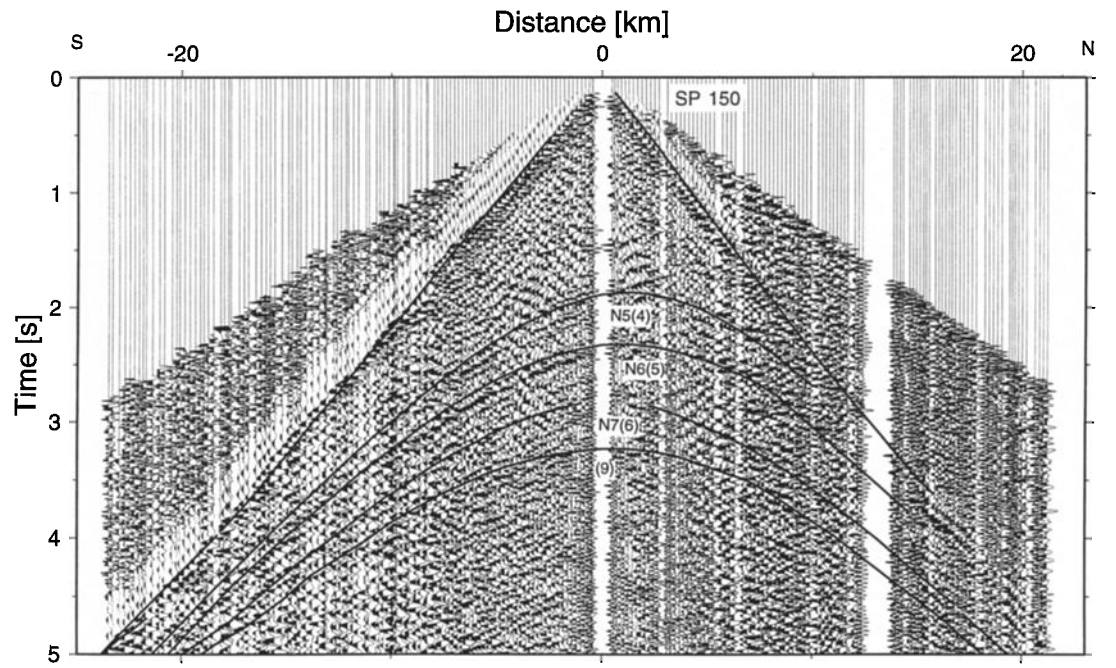

Figure 2f. SP150 displayed with unreduced travel time. See caption for Figure 2d for further explanation.

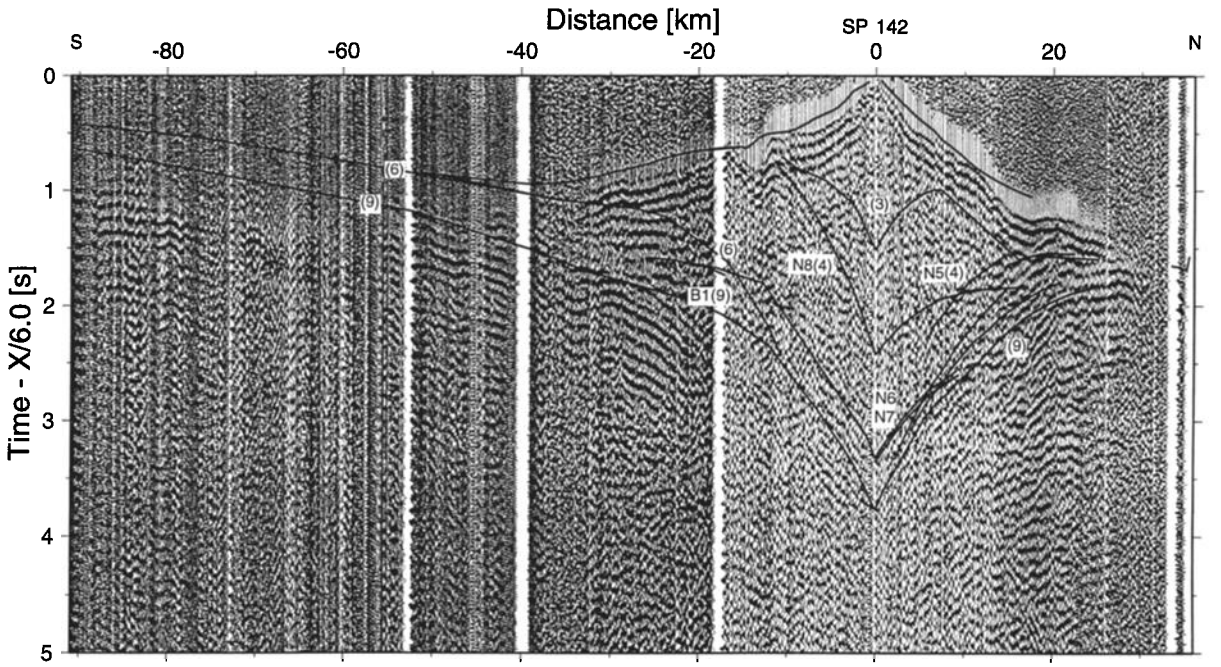

Figure 2g. SP142 displayed with reduced travel time. See caption for Figure 2c for further explanation. Asymmetry of phase N8(4), opposite to that of phases N5(4) and N6(5) of SP150, indicates a northward reflector dip.

in Plate 2) are estimated to be certain to <0.5 km and 0.15 km/s, respectively, in the upper crust and 1–2 km and 0.2–0.3 km/s, respectively, in the lower crust and mantle. Interface depths and velocities determined only by reflections (gray lines and gray numbers in Plate 2) are more uncertain. For example, on the North Slope between SP150 and SP189 (model coordinates 335 and 396 km), where all interfaces and velocities below layer 1 are determined by matching reflection hyperbolae, the estimated error is at least 1 km and 0.5 km/s, respectively. These estimates are obtained from attempting alternate models (Figure 3). For the Moho and sub-Moho reflectors, points of critical reflection and the distance interval along the boundaries controlled by both precritical and postcritical reflections are indicated (heavy solid dots and thick gray dashed and solid lines, Plate 2). For offset shots on the North Slope, SP149 and SP153 (model coordinates 444 and 487 km), where no close receivers were present, we have used local oil well control for interfaces and velocities (Plate 2 and Figure 1).

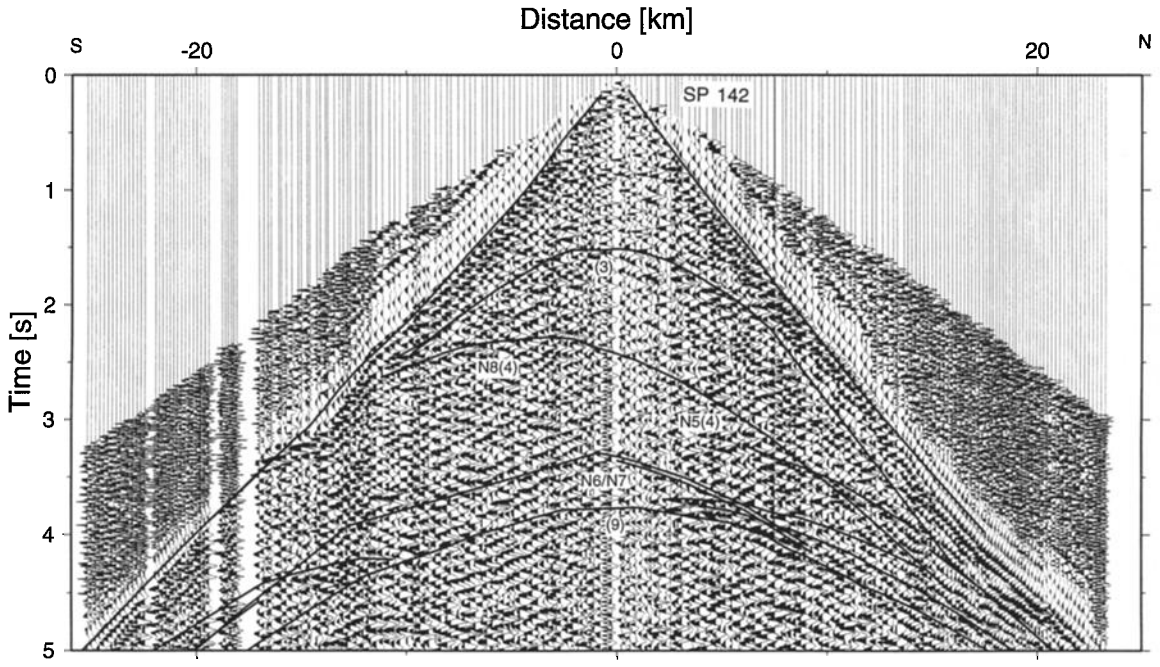

Figure 2h. SP142 displayed with unreduced travel time. See caption for Figure 2d for further explanation.

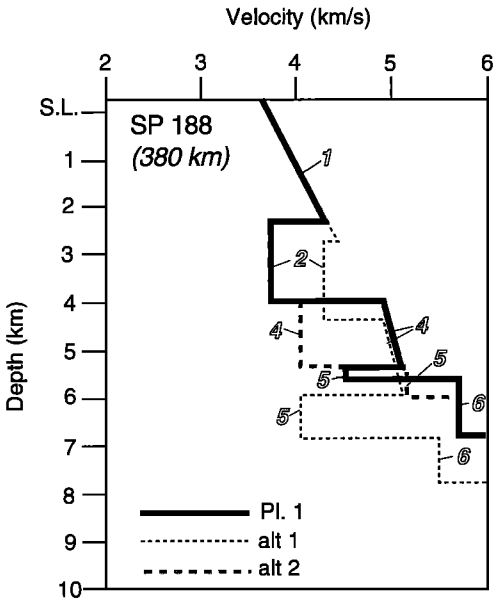

Figure 3. Velocity-depth curve at SP188 (model coordinate 380 km, Plate 2) along with alternate-model curves ("alt 1" and "alt 2"). Layer numbers are indicated (see Plate 2).

The velocity model (Plate 2) consists of 11 layers, some of which exist only in certain parts of the model. In the following discussion, these layers are discussed in order from top to bottom for, first, the Brooks Range and region to the south, where they can be compared with the starting, or inverse, model and second, the North Slope, where correlation with layers identified in the oil wells can be made.

Brooks Range, Koyukuk Basin, and Highlands southeast of the Koyukuk basin. The boundaries between layers 1 and 2 and between layers 2 and 4 are second-order discontinuities with velocities of 5.0 and 5.75 km/s, respectively (thin dashed black lines, Plate 2). Both agree within a few tenths of a kilometer in most places with the 5.0 and 5.75 km/s contours of the inverse model (faint, gray lines, Plate 2). Both contours lie within 1.25 km of the surface between the Doonerak antiform and the Wiseman thrust fault, i.e., through the Hammond and northern Coldfoot subterranes, and diverge from the surface and each other, producing lower velocity gradients, to the south and north.

The boundary between layers 4 and 6 is a velocity step that changes laterally from a minor step, generally less than 0.1 km/s, beneath the highlands southeast of the Koyukuk basin, the Koyukuk basin, and the southern Brooks Range to a moderate step in the northern Brooks Range, ranging from 0.15 to 0.3 km/s. In the southern Brooks Range, reflections seen at or near this boundary diverge consistently toward greater depth southward (e.g., reflectors C1–C3, Plate 2). In the northern Brooks Range, most reflections of zone A (A2, A3, and A4, Plate 2) lie at or below this boundary; reflection A1 lies above this boundary. From model coordinates 250 to 300 km, this boundary is interpreted (see below) as the boundary between NSS Ellesmerian and Franklinian ("basement") rocks. In contrast, from model coordinates 160 to 240 km, this boundary apparently represents a minor boundary within metamorphic and igneous rocks. Beneath the Ruby terrane near model coordinate 0 km, the layer 4/6 boundary may represent higher-velocity rocks at the base of a low-velocity(?) zone, but this low-velocity zone is constrained only by the offset shot at 0 km.

The layer 6/9 boundary was arbitrarily chosen to coincide with a series of prominent wide-angle reflections in the mid-crust, including the north dipping reflection at the top of zone E (reflector E1, Plate 2), a series of echelon reflections at the top of a zone of ramp-and-flat ("S"-shaped) reflections within zone D (reflectors D4–D10, Plate 2), and a couple of echelon reflections within zone B (reflectors B1 and B2, Plate 2). In matching first- and second-arrival travel times from large shots (e.g., Figures 4a–4d), the velocities of layer 6 could be reasonably well constrained (within ~0.15 km/s; see above); they range from 6.1 to 6.5 km/s and vary laterally and vertically.

Velocities within layer 9, the middle and lower crust, are constrained only by matching *PmP* hyperbolae (see Figures 4a–4g). Average velocities in this layer range from low on the North Slope (6.3–6.4 km/s) to intermediate beneath the highlands southeast of the Koyukuk basin and the Koyukuk basin (6.4–6.6 km/s) to high in the north central Brooks Range (6.7–6.8 km/s) in the region of thickest crust. These average velocities are constrained to perhaps within 0.2–0.3 km/s. Velocity gradients shown in the model for layer 9 are poorly constrained.

The Moho (top of layer 11 south of model coordinate 250 km and top of layer 10 north of 250 km) is constrained by precritical and postcritical reflections (*PmP*) and refractions (*Pn*) from the large shots (Figures 4a–4g). Moho depth changes from 33 km below sea level beneath the highlands southeast of the Koyukuk basin to 48 km below sea level beneath the highest part of the Brooks Range (the vicinity of Atigun Pass, Plate 2) and back to 32 km below sea level beneath the North Slope. *Pn* south of the crustal root is constrained from reversing shot points 120/70, 126, 132, and 139/140 (model coordinates 80/82, 148, 214, and 292 km, Plate 2; Figures 4a–4d) to be greater than 8.0 km/s; the best fitting model velocity is 8.2 km/s. *Pn* north of the crustal root is constrained chiefly from reversing shot points 126, 149, and 153 (model coordinates 148, 444, and 487 km, Plate 2; Figures 4b, 4f, and 4g) to be less than 8.0 km/s. The best fitting model velocity varies laterally from 7.6 km/s near the crustal root, where a relatively lower velocity is required to fit reversing *Pn* arrivals from SP126 and SP149, to 7.8 km/s farther north, where a relatively higher (but more poorly constrained) velocity is required to fit partly reversed *Pn* arrivals from SP153. In order to transmit *Pn* rays through the mantle north of the crustal root and back to the surface, a gentle negative velocity gradient is required in the mantle in this region of the model (see ray diagrams, Figures 4b, 4f, and 4g).

A sub-Moho reflector (*PumP*; *um* is upper mantle) is seen clearly from many shot points with bottoming points north of the crustal root, including shot points 132, 139/140, 189, and 149, (model coordinates 214, 292, 396, and 444, Plate 2; Figures 4c–4f). Such a reflection is not seen from shot points with bottoming points south of the crustal root (Figures 4a–4d). This reflector is constrained throughout by precritical reflections, some quite strong (Plate 2). For SP153, *PumP* arrivals are either superposed on *PmP* and *Pn* arrivals, or they are absent. The interpretation in Plate 2 assumes the former, as the sub-Moho boundary determined from shot points 132, 139/140, and 141 (not shown) projects northward from a depth of 54 km (model coordinate 300 km) to a depth of 44 km (model coordinate 390 km), where such superposition would be predicted. The velocity in the mantle above this reflection is constrained

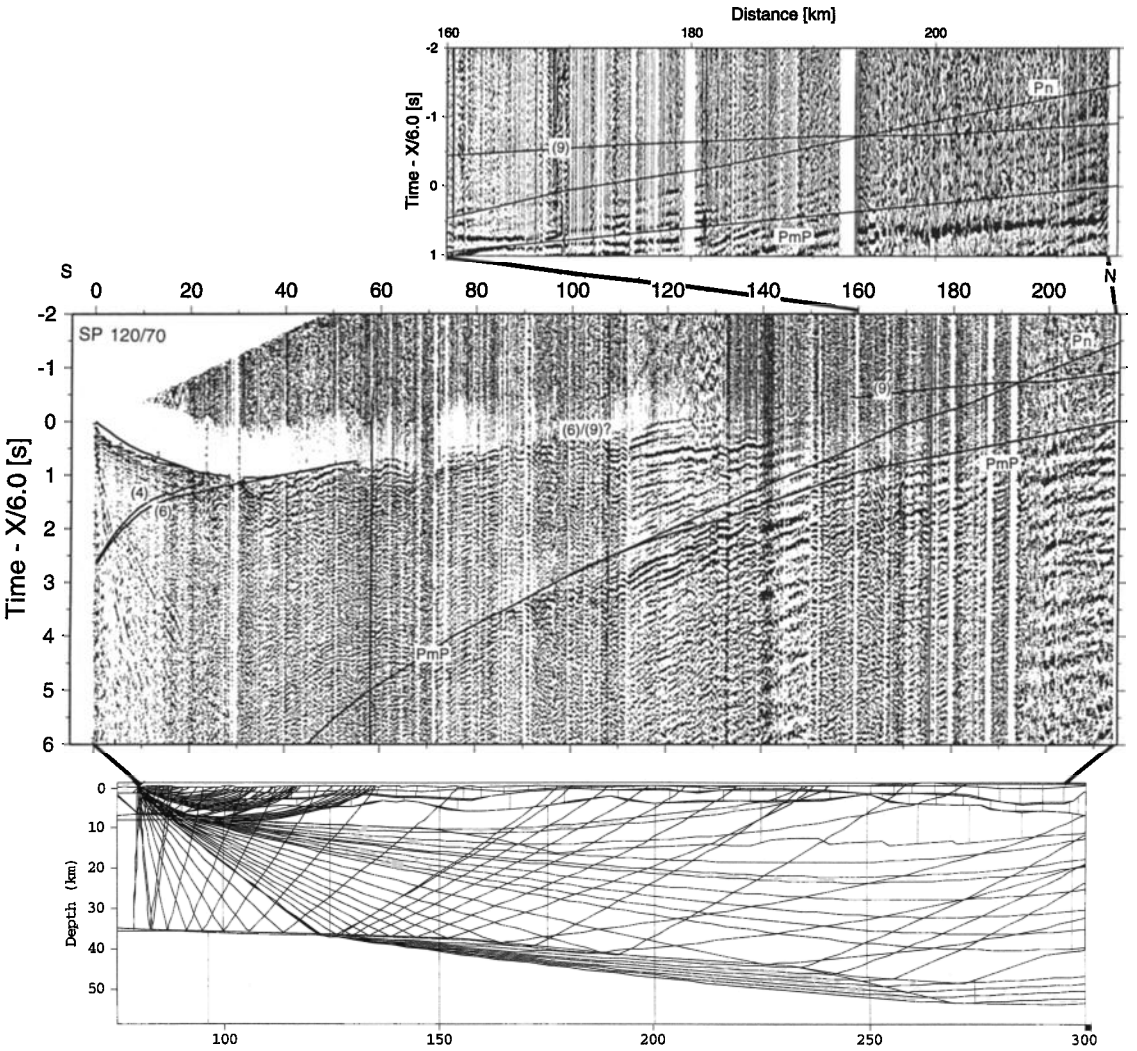

Figure 4a. Shot gather and ray diagram for SP120/70 showing model travel time curves for crustal and mantle phases. For shot gather, reduced travel time is displayed, and distances are given with respect to shot. Data are band-pass filtered and automatic gain controlled to enhance reflections. Model curves are labeled according to reflectors and/or layers generating phases (see Plate 2); layer numbers appear in parentheses: e.g., E1(9). Question mark appears next to layer number/(9) (6) on conspicuous phase for which model travel time curve could not be generated; presumably, this phase could be modeled as diffraction or head wave. *Pn* is mantle refraction; *PmP* is Moho reflection. Blowup of *Pn* arrival is shown. For ray diagram, VE = 1:1. This diagram covers approximately same range interval as data. Distance is given in model coordinates of Plate 2 for ease in relating to model. Vertical gray lines are velocity grid lines for each layer.

in its upper part by *Pn*, as described above, and in its lower part only by a projection of the required negative velocity gradient. The velocity beneath the reflector is unconstrained; it is assumed to match mantle velocity south of the crustal root.

An alternate explanation of the interpreted *PumP* arrival as a multiple was examined and rejected. We attempted to explain this arrival as *PmP* reverberating between the free surface and the layer 4/6 boundary (the shallowest, consistently strong reflector) near the receiving stations. Such a multiple recorded at model coordinates 275 to 300 km from SP189 (model coordinate 396) is 0.4 to 0.5 s late. Such a multiple recorded at model coordinates 375 to 400 km from SP139/140 (model coordinate 292 km) has the wrong moveout. Additional evidence that the interpreted *PumP* arrival is not a multiple is the vertical incidence image of an upper mantle reflective zone [*Wissinger et al.*, this issue]. The process of stacking vertical incidence reflections reduces multiples in the image because of their moveout.

North Slope. From shot points 150 to 189 (model coordinates 335 to 396 km), first arrivals die out at about 20-km offset (Figures 2c, 2e, and 4e), making it difficult to constrain the velocities of layers deeper than layer 1. Velocities of deeper layers are constrained by reflection hyperbolae, but, of course, the data do not describe perfect hyperbolae nor is the structure one-dimensional. Consequently, for this region of the North Slope it was necessary to construct several velocity models (Figure 3). All of these models fit the data about equally well, but interface depths and layer velocities differ among the models by as much as 1 km and 1.5 km/s, respectively, at 6 km depth (Figure 3). The model shown in Plate 2 is preferred over the alternate models (Figure 3, models "alt1" and "alt2"), because (1) its travel time fit is slightly better, (2) relative amplitudes

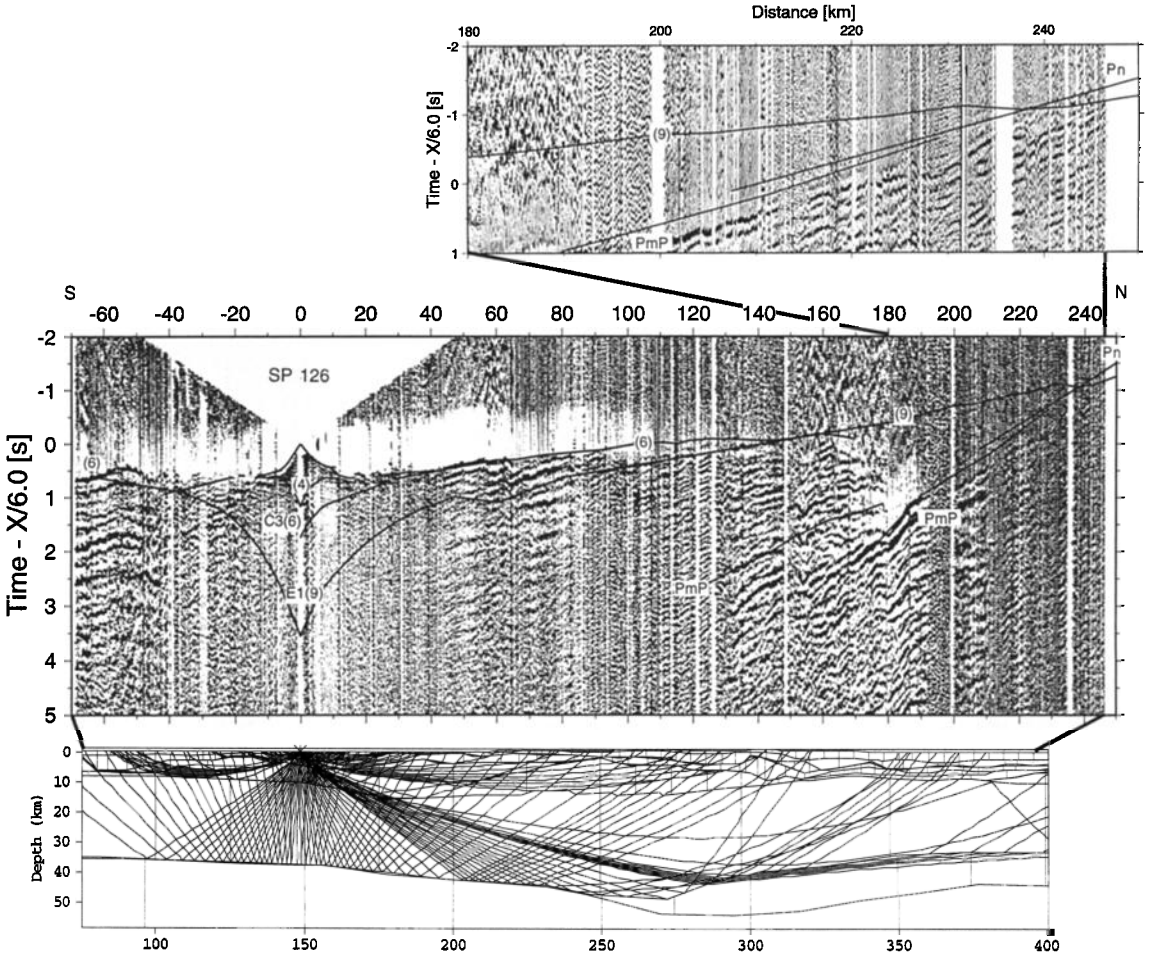

Figure 4b. Same as Figure 4a, except for SP126.

among the various reflections for this model agree better with synthetic amplitudes (for one-dimensional models, calculated using the WKBJ method (J. H. Luetgert, written communication, 1995)), and (3) its interface depths better agree with those projected from oil wells to the north. All models preserve the configuration of wide-angle reflections shown in Plate 2 (N1–N7).

From shot points 189 to 153 (model coordinates 396 to 487 km), no seismic receivers were present (see Plate 1), so the shallow velocity structure is controlled exclusively by oil-well data (Plate 2 and Figure 1). Below 4 km depth, the structure is controlled by unreversed arrival branches from shot points 149 and 153 (Figures 4f and 4g).

The following observations can be made from the preferred model (Plate 2):

1. South of SP189, layer 1 is chiefly Upper Cretaceous Brookian sedimentary rocks with southward increasing velocities and positive velocity gradients (0.25–0.6 s^{-1}). North of SP189, layer 1 includes both Upper Cretaceous and Cenozoic Brookian rocks with lower velocities than to the south and a higher velocity gradient (~1 s^{-1}), determined from interval-velocity measurements in the oil wells (Figure 1). North of SP149, layer 1 includes at its top as much as 0.5 km of ice-rich permafrost, with velocities averaging 2.5–3.5 km/s.

2. South of SP189, layer 2 has a small or negative velocity gradient and may constitute a small negative velocity step from layer 1. This feature serves to terminate refraction branches generated in layer 1, as observed in the data (Figures 2c, 2e, and 4e). North of SP189, layer 2 has similar properties, as determined from oil well data (Figure 1).

3. North of model coordinate 355 km, layers 4 and 5 are uncertain in velocity and thickness as indicated by the alternate models (Figure 3).

4. Between model coordinates 295 and 345 km, layer 4 constitutes an asymmetric synform with steeper boundaries, a greater thickness and a higher velocity in the south limb (Plate 2). The velocities of layers 3 and 4 are constrained by refractions and are consistent with carbonate rocks of the Lisburne Group (see Interpretation section, below). Although not constrained by refractions, the velocity of layer 5 appears similar to that of layer 4.

5. Between model coordinates 330 and 400 km, layer 6 has a poorly constrained velocity of 5.5–5.7 km/s. It projects northward into a layer of similar velocity penetrated by several oil wells and identified as carbonate rocks of the Lisburne Group.

6. Layer 8 is penetrated by an oil well at model coordinate 492 and identified as Franklinian argillite ("basement") with a velocity of 4.94 km/s. Unreversed first-arrival branches from both shot points 149 and 153 require higher-velocity basement to the south (Figures 4f and 4g). The way we have chosen to model basement (layers 8 and 9) is nonunique but does explain two basement phases observed from SP149 (Figure 4f, phases 8 and 9).

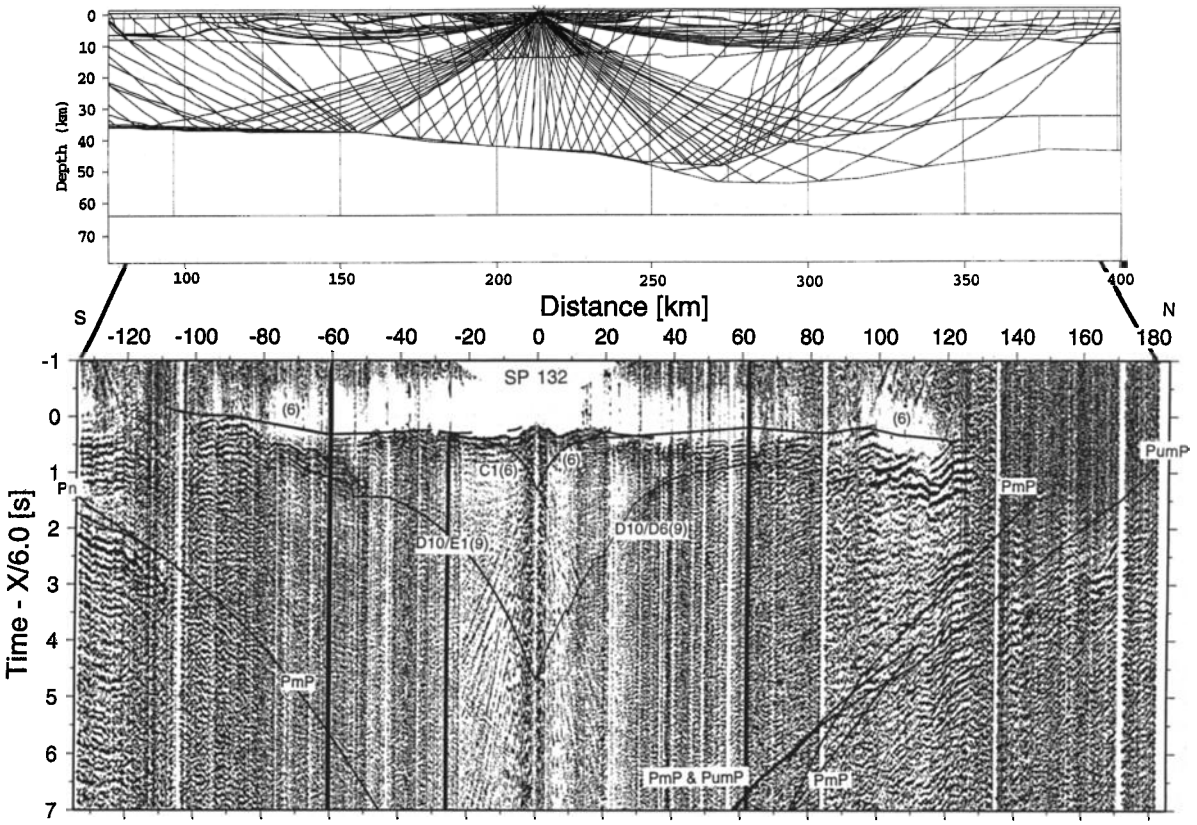

Figure 4c. Same as Figure 4a, except for SP132. *PumP* is reflection from within upper mantle.

Laboratory Rock Velocities

Samples of representative rocks from each terrane or subterrane in the highlands southeast of the Koyukuk basin, the Koyukuk basin, the Brooks Range, and the North Slope were collected in order to make measurements of seismic velocity and density in the laboratory (Table 2). Velocities were measured as a function of confining pressure in three mutually perpendicular directions for each rock using the pulse transmission technique described in detail by *Christensen* [1985]. The velocities summarized in Table 2 at 50, 100, and 200 MPa are averages of the three measurements and thus represent approximate isotropic averages.

Rocks with the highest velocities (6.4–6.5 km/s at 100 MPa) include the metabasalts and metagabbros of the Angayucham terrane, Slate Creek/Prospect Creek subterrane, and North Slope subterrane, and marble (Skajit Limestone) of the Hammond subterrane. Rocks with the lowest velocities (4.6–5.3 km/s at 100 MPa) include a phyllite of the Ruby terrane and siltstones of the North Slope subterrane.

In order to compare laboratory velocities with model (or "field") velocities the percentage of each rock type in a terrane or subterrane along the transect was estimated, and a weighted average laboratory velocity was calculated. The EMS is divided into two parts, as these percentages change across the Toyuk thrust fault [see *Moore et al.*, this issue]. Estimated average laboratory velocities were calculated at 50, 100, and 200 MPa and plotted along with representative model velocity-depth curves for each terrane or subterrane (Table 2 and Figure 5).

For most terranes and subterranes the agreement between laboratory and model (or "field") velocities is generally good at about 4 km depth, but "field" velocities are low at about 2 km depth and high at about 8 km depth. (Note that each "field" curve has an error zone about it of approximately 0.15 km/s, see above.) Lower "field" velocities at 2 km depth might be explained by the presence of megascopic fractures in the field at shallow depth, but higher "field" velocities at 8 km depth suggest a change in rock composition from that calculated in the average (see Table 2). Accordingly, in the interpretive cross section (Plate 3), most terranes and subterranes are shown to be underlain at varying depths below 4 km by different terranes (see Interpretation section, below). The Angayucham terrane (Figure 5c) is different from other terranes in that "field" velocities at both 2 and 4 km depth are lower than calculated average laboratory velocities, leading one to speculate that perhaps volcanic breccia zones, common in ophiolitic terranes, may be present at shallow depth (see Interpretation section).

NSS Franklinian and Ellesmerian rocks are exposed in the Doonerak window and also east of our profile (Plate 1). Surface geologic relations suggest these rocks are present beneath the profile northward from approximately model coordinate 240 at depths that begin anywhere from a few kilometers to 10 km. They may be represented in the deeper parts of the velocity-depth curves in the vicinity of the Doonerak antiform (see Figures 5i–5k). The northern "field" curve (Figure 5k) agrees well with calculated laboratory velocities for these rocks, but the southern two curves (Figures 5i and 5j) are high compared to these calculated velocities.

Interpretation

On the basis of surface geology, laboratory and model velocities, and reflection character the interpretive cross section

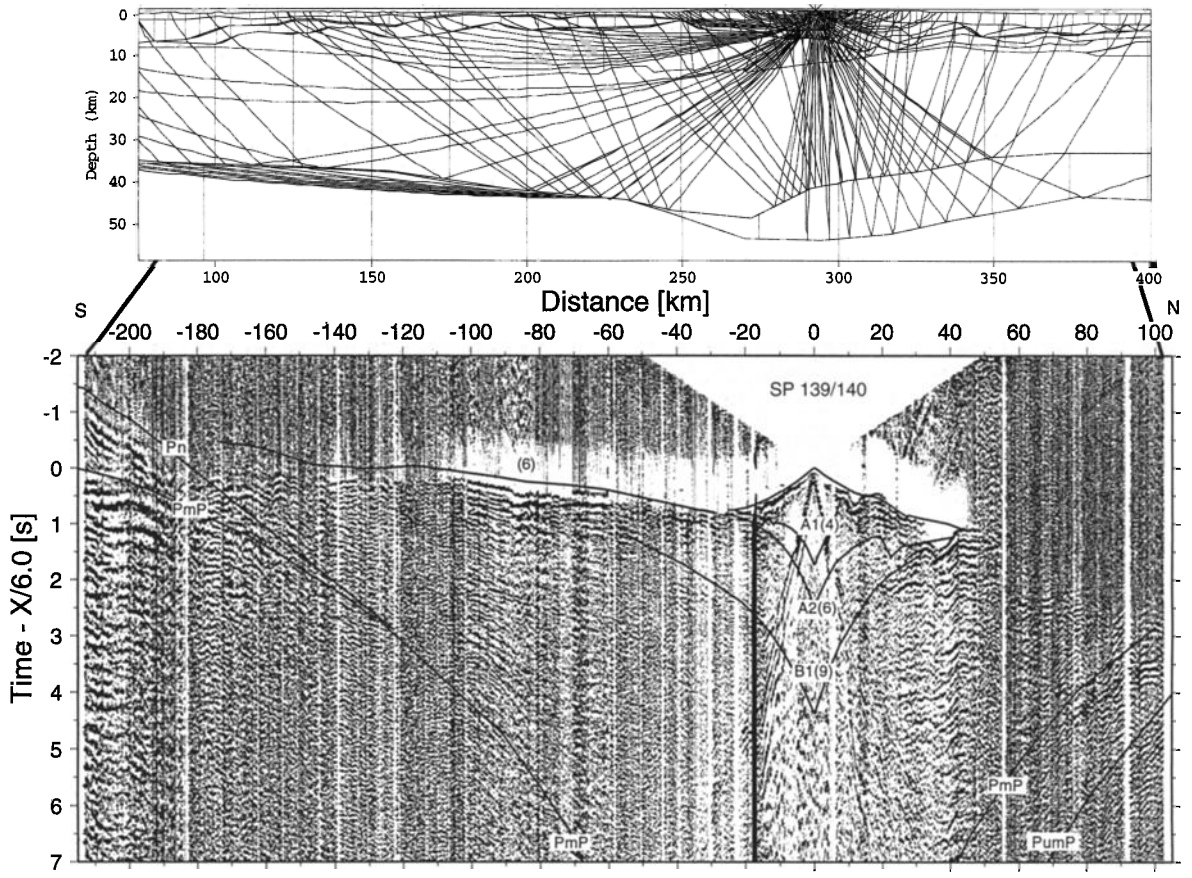

Figure 4d. Same as Figure 4a, except for SP139/140.

(Plate 3) is drawn. We discuss first the Brooks Range and then the North Slope.

Brooks Range

The following discussion proceeds from north to south through the terranes and subterranes exposed at the surface in the Brooks Range and then downward through the zones (A–F) imaged beneath the Brooks Range.

Endicott Mountains subterrane. Rocks of the EMS are interpreted to constitute layers 1 and 2 and the upper part of layer 4 between the sub-Endicott Mountains thrust fault and the Atigun Gorge thrust fault (model coordinates 257 and 302 km, Plates 2 and 3). The EMS consists of generally younger rocks from south to north, with chiefly Hunt Fork Shale in the south and chiefly Kanayut Conglomerate (conglomerate, sandstone, and shale) in the north (Table 2 [e.g., *Moore et al.*, this issue]). The Lisburne Group of the EMS crops out only in the northernmost exposures of the EMS, north of model coordinate 295 km. Model velocities at 4 km depth compare well with average laboratory velocities for this terrane, as discussed above (Figures 5g and 5h and Table 2).

The anomalously high-velocity body at the north end of the EMS (5.9–6.1 km/s, centered at model coordinate 300 km, Plate 2) corresponds spacially with outcrops of imbricated and folded horses of carbonate rocks of the Lisburne Group [*Moore et al.*, this issue; *Wallace et al.*, this issue]. The high-velocity body extends from near the surface to 7 km depth. Laboratory velocities for samples of carbonate rocks from this location range from 5.7 to 6.2 km/s (at 50–200 MPa, respectively, Table 2) and thus match model velocities for the high-velocity body quite well. Reflections within this body dip gently northward (~20°; see discussion of the synformal structure above), suggesting overall northward dips for these interpreted carbonate horses (or for some boundaries within this assemblage of horses). The identity of these interpreted horses, whether they belong entirely to the EMS or NSS or partly to each, is unknown. We made the body chiefly EMS Lisburne Group based on the fact that it is located immediately beneath outcrops of EMS Lisburne Group. Alternate interpretations would include making the high-velocity body chiefly NSS Lisburne Group (as in work by *Fuis et al.* [1995]) or even NSS Franklinian basement rocks; however, there is no field evidence to support a basement uplift at this location.

North Slope subterrane (exposures in the Doonerak window). Ellesmerian and Franklinian rocks of the NSS are exposed in the Doonerak window, ~5 km west of our transect; the Doonerak antiformal axis crosses our profile near model coordinate 240 km [e.g., *Moore et al.*, this issue] (Plates 1–3). In Figures 5i–5k, average laboratory velocity for NSS Ellesmerian and Franklinian rocks are compared with model velocity-depth curves at three locations near the antiformal axis, where NSS rocks may be present at depth. It is clear that at 240 and 249 km, neither NSS Ellesmerian nor Franklinian rocks match model velocities. However, by increasing the percentage of greenstone (sample 84, Table 2) over that estimated for outcrops in the Doonerak window (20%), one could easily match the model curves at those locations with NSS Franklinian basement rocks. At 261 km, one could interpret either NSS Elles-

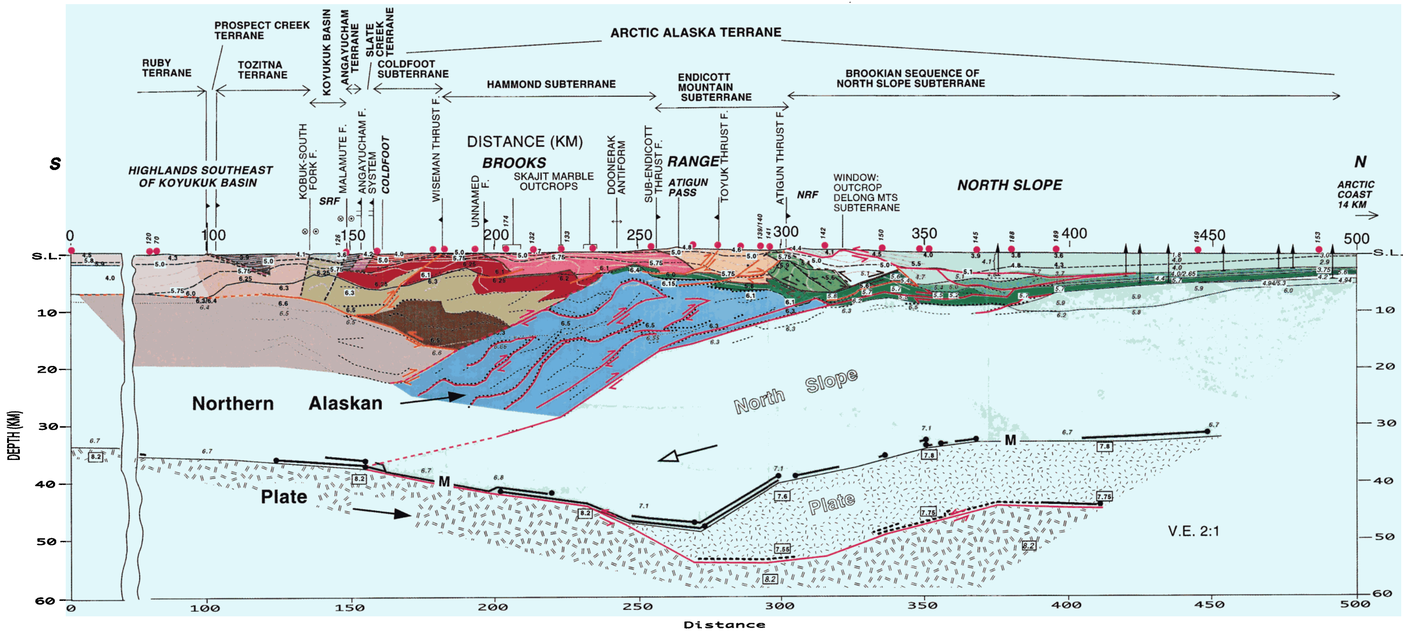

Plate 3. Geological interpretation of Plate 2. See explanation for description of geological units and most symbols. Faults shown at top of model are symbolized as follows: tooth, upper plate of thrust fault; double line, downthrown plate of normal fault; circled cross and circled dot, motion away and toward, respectively, on strike-slip faults. SRF, southern range front; NRF, northern range front. VE = 2:1.

EXPLANATION FOR MAP (PLATE 1) AND CROSS SECTION (PLATE 3)

Brookian sequence and rocks of Koyukuk basin

- Terrigenous clastic sedimentary rocks (Cenozoic).*
- Terrigenous clastic sedimentary rocks (Cretaceous).
- Volcanic rocks (Cretaceous).*

North Slope subterrane (exclusive of Brookian sequence)

- Post-Lisburne Group sedimentary rocks (Perm.-L. Cret.) of Ellesmerian sequence. Chiefly shale and sandstone.**
- Lisburne Group and older rocks (Miss. and Penn.) of Ellesmerian sequence. Chiefly limestone with shale, sandstone, and conglomerate.
- Franklinian sequence (pre-Miss.). Metasedimentary, metavolcanic, and plutonic rocks. Light blue color** denotes rocks largely undeformed in the latest Jur. to present Brooks Range orogeny.

Endicott Mountains subterrane

- Post-Lisburne Group sedimentary rocks of Endicott Mts. subterrane (Perm.-L. Cret.).** Includes sedimentary rocks of Delong Mts. subterrane.
- Lisburne Group (Penn. and Miss.). Chiefly limestone.**
- Endicott Group (Miss. and Upper Dev.). Chiefly sandstone, shale, and conglomerate. (On map*, all EMS shown as flesh color.)

Hammond subterrane

- Phyllite and marble (Prot?-Dev.).

Coldfoot subterrane

- Schist and orthogneiss (Prot?-Dev.).

Slate Creek and Prospect Creek terranes

- Phyllonite and melange.

Angayucham and Tozitna terranes

- Metabasite, chert, and siliceous sedimentary rocks (Dev.-Jur.).

Delong Mountains subterrane

- Chert, sandstone and shale (Jurassic and L. Cret.).* On cross section**, combined with Post-Lisburne Group sedimentary rocks of Endicott Mts subterrane.

Ruby terrane

- Metasedimentary and metavolcanic rocks (Prot?-Dev.). Light gray color** denotes low-velocity zone.
- Plutonic rocks (Cretaceous).**

Unknown terranes

- With intermediate velocity.
- With intermediate to high velocity.
- With north-dipping reflections.

Symbols

- Major faults*; arrows denote relative motion of strike-slip faults, teeth denote upper plate of thrust faults,and hachures denote hanging wall of normal fault. Dashed where concealed.
- Major faults**; relative age indicated by color: red, youngest; brown, oldest; arrows indicate relative motion of faults (see caption of Plate 2 or 3 for explanation of faults symbols shown at the surface); dashes indicate relatively less certainty in attitude or existence.
- Shotpoint; numbers** shown for shotpoints discussed in text.
- Oil well.**
- Seismic boundary**; solid black and finely dashed gray lines, first-order discontinuities; seismic P-wave velocity above and below in km/s. Velocities in italic light gray font and boundaries in light gray, less certain. Long-dashed black lines, second-order discontinuities; velocity on discontinuity in km/s.
- Contour of seismic P-wave velocity**; Interval, 0.25 km/s; unlabeled.
- Wide-angle reflections**; prominent; moderate to weak; studied in preliminary fashion only
- On Moho and sub-Moho reflectors**, black dot is point of critical reflection; solid gray line represents bottoming points of post-critical reflections; dashed gray line represents bottoming points of pre-critical reflections.

* Map only
** Cross section only

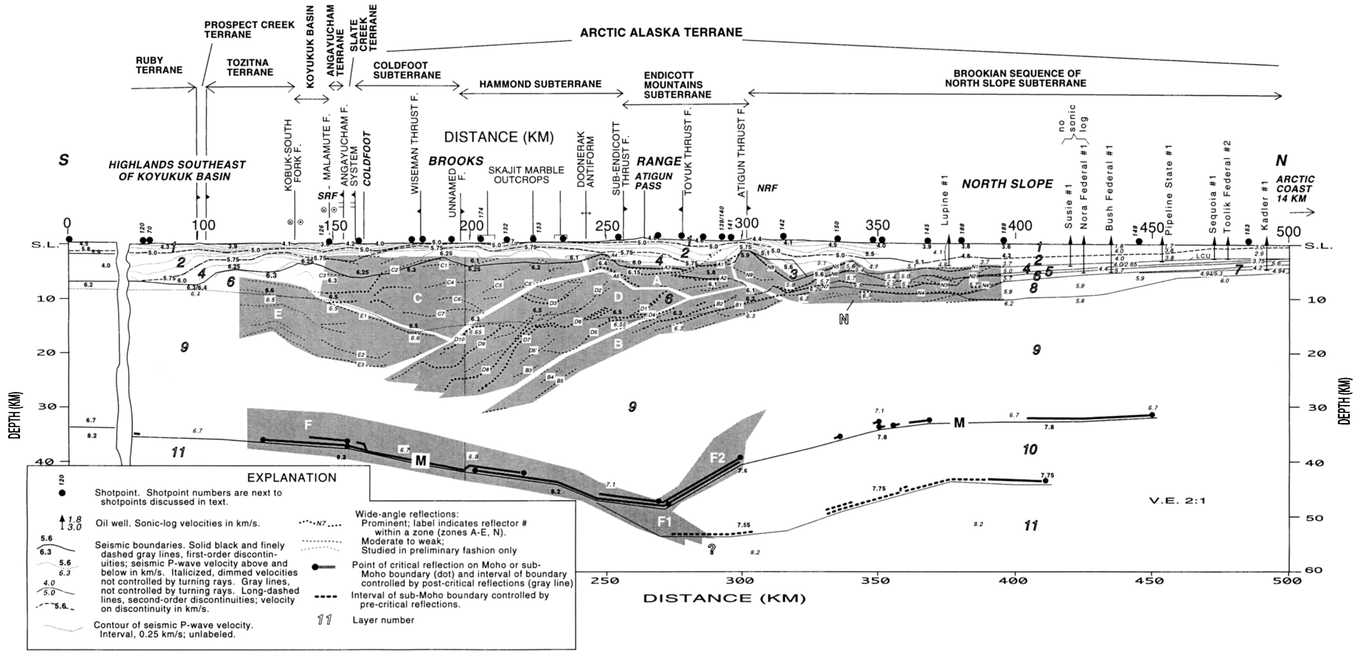

Plate 2. *P* wave velocity and reflectivity model from this study. See explanation for description of most symbols. Faults shown at top of model are symbolized as follows: tooth, upper plate of thrust fault; double line, downthrown plate of normal fault; circled cross and circled dot, motion away and toward, respectively, on strike-slip faults. SRF, southern range front; NRF, northern range front. VE = 2:1. Gray regions with white letters indicate zones of reflections (see Table 1).

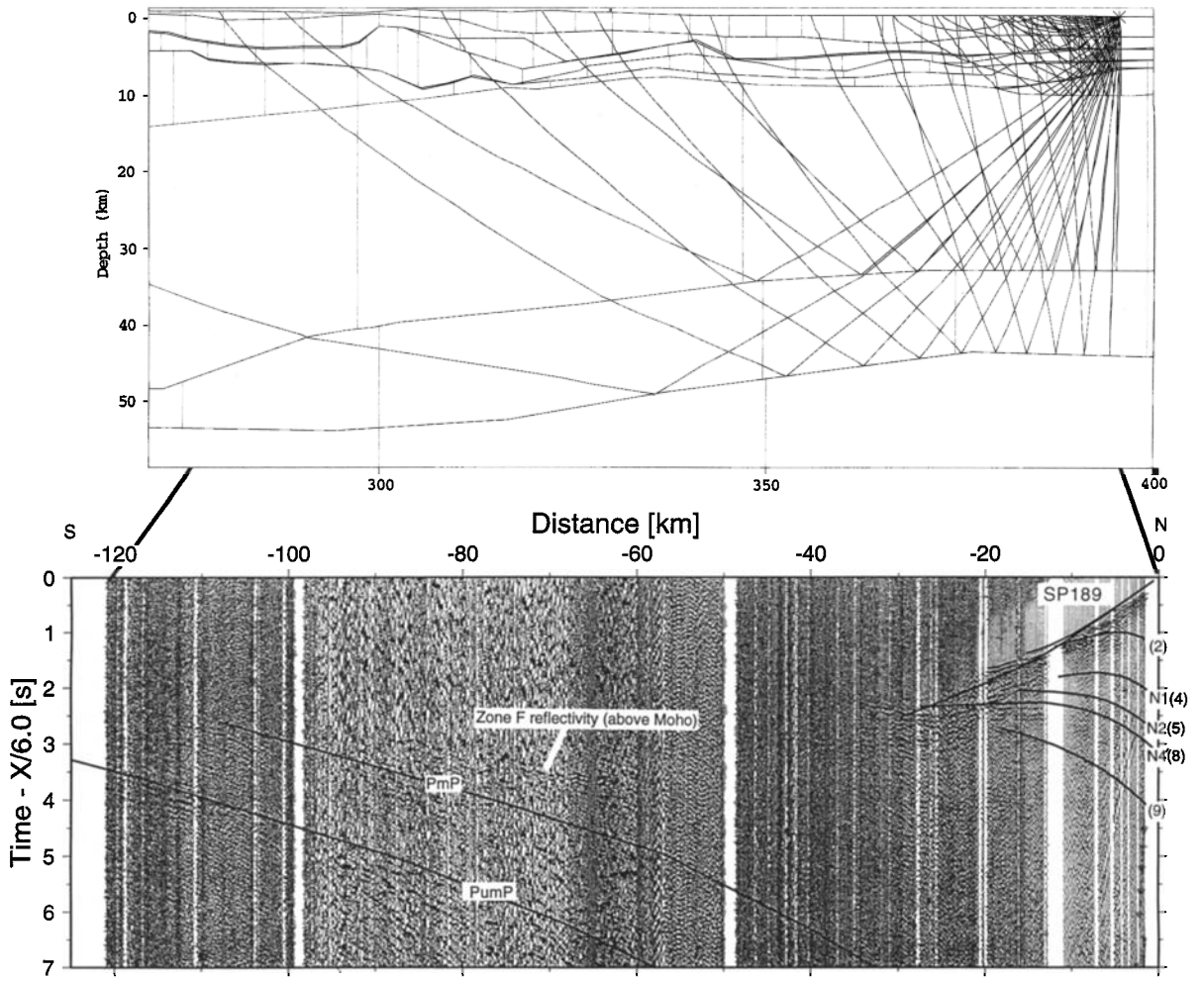

Figure 4e. Same as Figure 4a, except for SP189.

merian or Franklinian rocks at depth. Our interpretation (Plate 3) is that NSS Ellesmerian rocks, chiefly carbonate rocks of the Lisburne Group, are present at depths where model velocities fall in the range 5.7–6.0 km/s (see samples 82 and 88 at 50–100 MPa, Table 2), i.e., in the bottom part of layer 4 from model range 250 to 300 km (Figures 5j and 5k and Plate 3). We interpret layer 6 to be Franklinian basement rocks in the same model range interval. An alternative interpretation would make the upper part of layer 6 NSS Lisburne Group in the range interval 261–300 km.

Hammond subterrane. On the basis of surface geologic relations and on the agreement between model and average laboratory velocity for this subterrane to as much as 4 km depth (Figure 5f), the Hammond subterrane is interpreted to constitute layers 1, 2, and 4 between the unnamed fault at model coordinate 197 km and the sub-Endicott thrust fault at 257 km (Plates 2 and 3). Unfortunately, the similarity of average laboratory velocity between this and other nearby subterranes makes this interpretation highly nonunique (see Table 2).

Coldfoot subterrane. As was the case for the Hammond subterrane, surface geologic relations and agreement between model and average laboratory velocity for this terrane to as much as 4 km depth (Figure 5e), lead us to interpret this subterrane to constitute approximately layers 1, 2, and 4 between the Angayucham fault system and the unnamed thrust fault at its northern boundary. On the basis of surface geologic relations alone, this subterrane is extended northward beneath the Hammond subterrane (in layer 6) to nearly model coordinate 240 [see *Moore et al.*, this issue]. Intermediate model velocity in layer 6 (6.3–6.5 km/s) from model range 150–190 (higher than the average laboratory velocity for the Coldfoot terrane (Figure 5e)) leads us to postulate the existence of unknown terranes for most of layer 6 in this region.

Slate Creek, Angayucham, and Koyukuk terranes. The Slate Creek subterrane and Angayucham terrane are underlain by a subhorizontal wide-angle reflection at 2–3 km depth (Plate 2) and are interpreted to be truncated at that depth. A comparison of average laboratory and model velocity at 4 km depth indicates the Slate Creek subterrane could be interpreted to extend deeper (Figure 5d). On the other hand, the Angayucham terrane must contain much lower-velocity rock than estimated at the surface for all depths above about 5 km (Figure 5c). The presence of the Coldfoot subterrane beneath these two terranes is speculative. The Koyukuk terrane is clearly underlain by an unknown terrane at shallow depth based on the poor match of average laboratory velocity for this terrane and model velocity at 4 km depth (Figure 5b). (Future modeling of magnetic data along our profile could modify our interpretation of the depth extent of these three terranes, especially the Angayucham terrane, which is quite magnetic.)

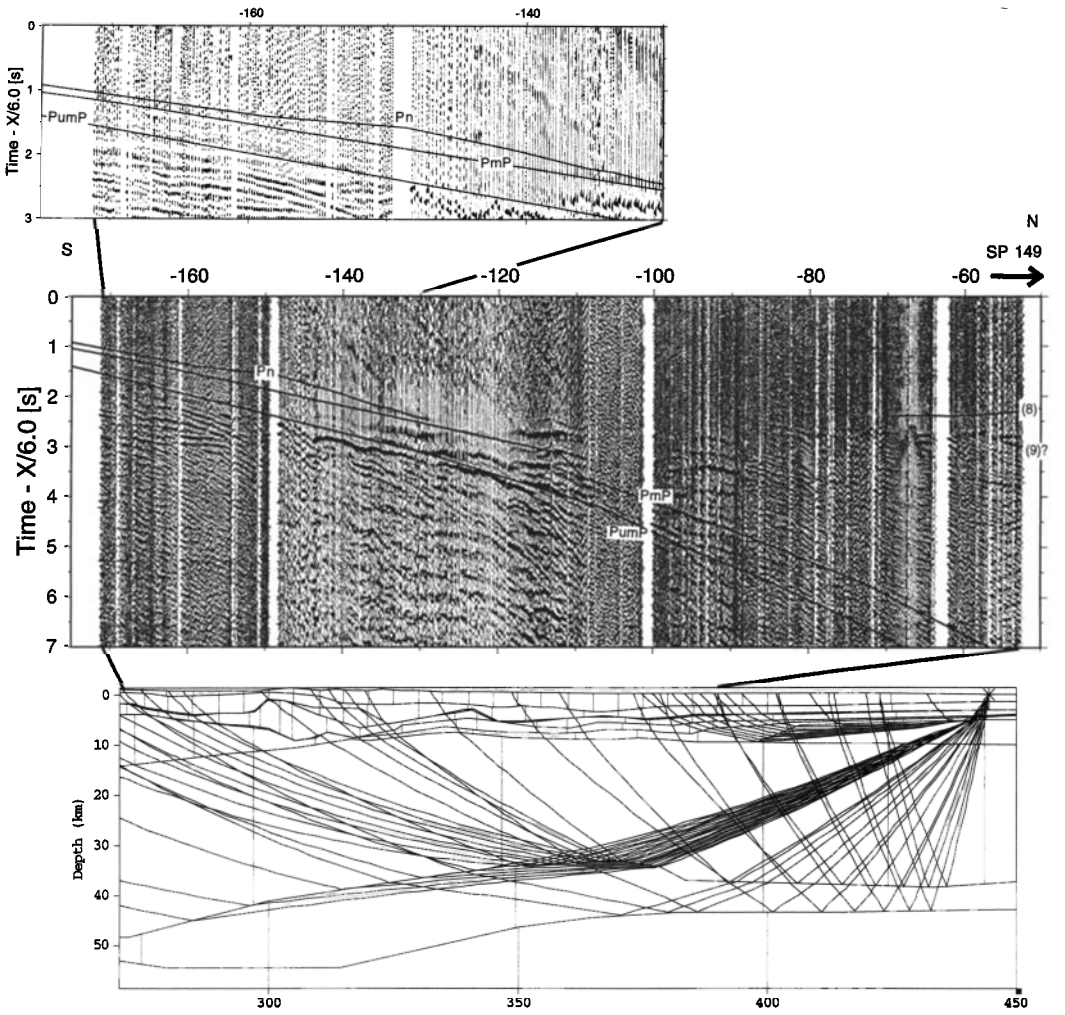

Figure 4f. Same as Figure 4a, except for SP149. Moho structure differs from that of Plate 2 northward of model coordinate 370 km (*PmP* critical point for SP149); in this region, deepening of Moho was necessary to enable match to precritical *PmP*.

Ruby terrane. The similarity of average laboratory and model velocities to nearly 8 km depth suggests that this terrane extends to at least this depth with a composition similar to that at the surface (Figure 5a).

Zone A. Located in the northern Brooks Range, zone A contains strong, parallel to echelon, subhorizontal wide-angle reflections that are gently arched near the Doonerak antiformal axis (250 km, Plate 2 and Table 1). This zone includes the top part of layer 6 from 240 to 295 km and all of layer 4 from 280 to 295 km (Plate 2). With one exception, the strongest reflections in this zone lie at or near the layer 4/layer 6 boundary, interpreted as the contact between Ellesmerian rocks and Franklinian basement rocks (Plate 3). For comparison, strong vertical incidence reflections are observed in many places along this same contact on the North Slope (see line C of *Oldow et al.* [1987]). However, strong vertical incidence reflections are also observed within Ellesmerian and Brookian rocks on the North Slope (see Richfield Oil Line AS2 of *Mull et al.* [1987] and *Gryc* [1988]). (Note that the strongest reflections on the North Slope are the Ellesmerian/Brookian contact, or Lower Cretaceous unconformity (LCU), the top of the Triassic sequence (top of Sag River and Shublik Formations) and, in places, the basement. The top of the Lisburne Group is not strongly reflective on the North Slope, although it becomes more reflective in the northern foothills of the Brooks Range.)

Fuis et al. [1995] interpreted the Lisburne Group to be coextensive with zone A, whereas we interpret a bit more complexity. Here the Lisburne Group coincides with zone A only where velocities are less than 6.0 km/s (280–295 km, Plates 2 and 3).

Zone B. Located in the northern and central Brooks Range, zone B contains strong, linear, south dipping, echelon reflections (Plate 2 and Table 1). This zone is interpreted as thrust horses of NSS Franklinian rocks. *Fuis et al.* [1995] interpreted the basal decollement of the Brooks Range at the base of zone B (subhorizontal dashed and queried red line at 15 to 17 km depth, Plate 3). In their interpretation, faults bounding thrust horses soled into the basal decollement that was itself not necessarily visible. In this study we interpret the basal decollement at a strong reflection within zone B (B1, Plate 2) and query faults along or bounding the weaker reflections below B1. Certainly, arguments could be made in favor of either interpretation. Except for this zone of uncertainty between the two possible locations of the basal decollement, wide-angle reflections are present only above the decollement and are absent between the decollement and the Moho. Al-

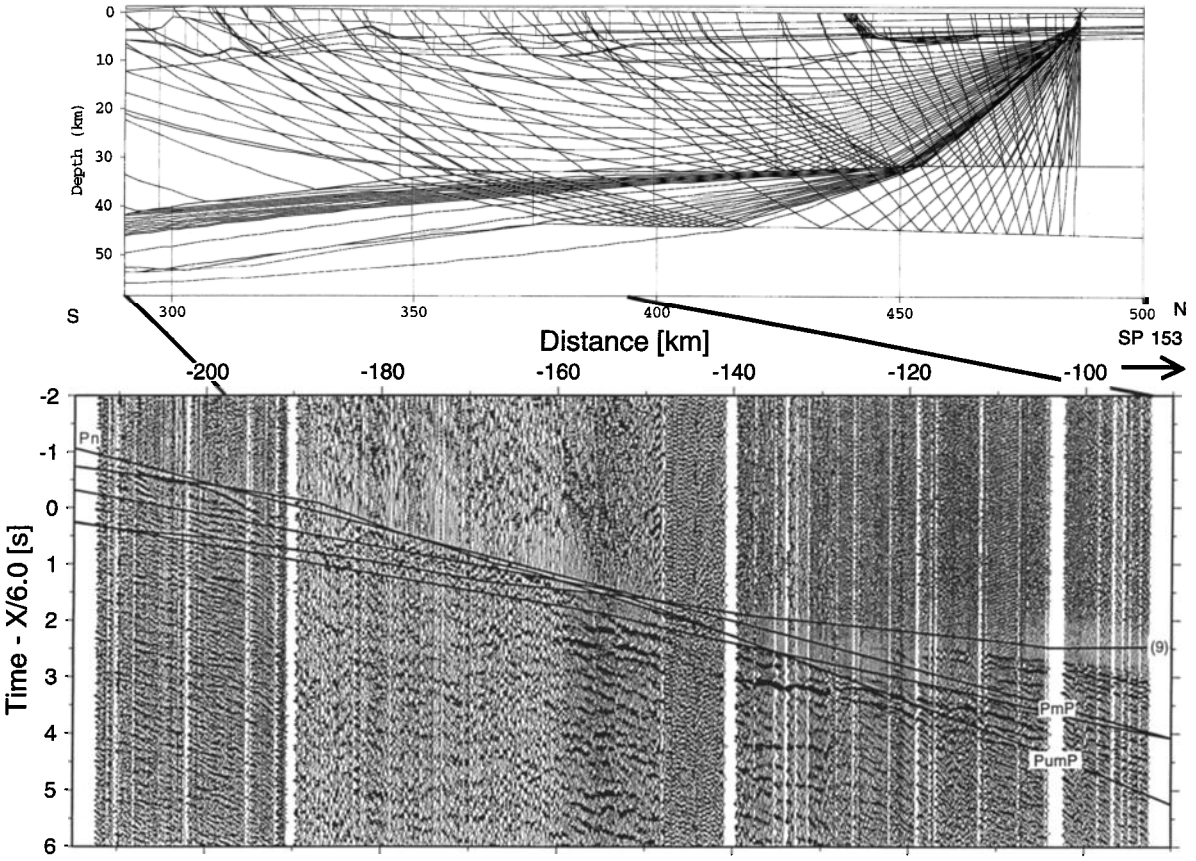

Figure 4g. Same as Figure 4a, except for SP153.

though model velocity in this zone (6.3 ± 0.15 km/s) is consistent with a mixture of Franklinian rocks similar to those exposed in the Doonerak Window (see Table 2), it is also consistent with many other rocks, including (marginally) carbonate rocks of the Lisburne Group.

Zone C. Located in the central and southern Brooks Range, zone C contains moderate to weak, flat to gently south or north dipping reflections (Plate 2 and Table 1). Intermediate velocities in this zone are interpreted to represent the Coldfoot subterrane and unknown intermediate-velocity terranes. The configuration of seismic velocity contours in the upper part of zone C (Plate 2) suggest northward vergence, but the shapes and thicknesses of interpreted rock bodies are poorly constrained.

Zone D. Cresting beneath the axis of the Doonerak antiform, zone D contains distinctive, strong reflections that have curved to ramp-and-flat geometries, with moderate south dips on the ramps (Plate 2 and Table 1). Zone D is interpreted as thrust horses of Franklinian basement rocks, as is zone B. The thrust horses of zones B and D are interpreted to be latest Cretaceous to Cenozoic in age, because cooling, interpreted as uplift, of the Doonerak antiform occurred at 65–70 Ma and at 24 ± 3 Ma [*O'Sullivan et al.*, 1997]. However, the seismic image of zone D may be complicated by older structures.

Zone E. In the middle crust beneath the highlands southeast of the Koyukuk basin, the Koyukuk basin, and the southern Brooks Range, zone E contains moderate to weak wide-angle reflections that dip gently northward. Multiple interpretations of zone E are possible, because it can not be tied to outcrop. *Grantz et al.* [1991] proposed north dipping panels of basement rocks in this region, from which the overlying Mesozoic terranes of the Brooks Range were stripped during northward thrusting. Alternatively, the reflections of zone E may represent detachment faults that originated during extension in the southern Brooks Range. Finally, as interpreted in Plate 3, this zone may represent the top of a tectonic wedge of Ruby(?) terrane rocks. Although wide-angle reflections of zone E extend across the deep projections of the Cretaceous Kobuk-South Fork and Malamute faults, they cannot clearly resolve truncation of these faults, as interpreted in Plate 3.

Zone F. Zone F is a 2-s-thick (~6 km) zone of vertical incidence reflectivity largely above the Moho that bifurcates between model coordinates 250 and 275 km, with a lower branch below the Moho (Plate 2 and Table 1) [see also *Wissinger et al.*, this issue]. Zone F is not clearly seen in the wide-angle reflection data (exception Figure 4e), but the Moho, which is seen in the wide-angle data, falls within and near the base of this zone. The interpretation shown in Plate 3 is only one possible interpretation, whereby the Moho between model coordinates ~150 and 250 km is a gently north dipping fault that continues as the sub-Moho reflector northward of 250 km. The interpretation of a fault in this position is supported by the resolvable difference in mantle velocity north and south of model coordinate 250 km. The basal decollement of the Brooks Range is interpreted as the upper fault of an interpreted tectonic wedge lying above the postulated Moho/sub-Moho fault.

The sub-Moho reflector in our model (Plate 2) reaches a maximum depth of about 54 km between model coordinates

Table 2. Laboratory Rock Velocities and Estimates of Average Velocities of Terranes and Subterranes

Terrane	Sample†	Percent of Outcrop Along Transect	Density, kg/m^3	V_{ave}, km/s			Weighted Average of Laboratory Velocities, km/s					
				50 MPa	100 MPa	200 MPa	50 MPa	Weighted Error	100 MPa	Weighted Error	200 MPa	Weighted Error
Ruby	67-phyllite (schist)	20	2405	4.366	4.600	4.861	5.283	0.403	5.521	0.375	5.754	0.356
	68-quartzite	20	2630	5.848	5.895	5.950						
	69-granite	50	2574	5.241	5.563	5.893						
	marble + metabasite*	10		6.2	6.4	6.45						
	total	100										
Koyukuk	92-conglomerate	30	2668	5.762	5.839	5.918	5.734	0.029	5.827	0.023	5.885	0.030
	sandstone*	40		5.7	5.8	5.85						
	shale*	30		5.75	5.85	5.9						
	total	100										
Angayucham	87-greenstone (Narvak panel)	32	2935	6.248	6.361	6.485	6.257	0.056	6.355	0.042	6.451	0.042
	94-metabasalt (Narvak panel)	32	2949	6.339	6.410	6.487						
	96-metabasalt	32	2947	6.229	6.338	6.431						
	argillite, chert, carbonate*	4		5.9	6.0	6.05						
	total	100										
Slate Creek/ Prospect Creek	101-metagraywacke	30	2652	5.485	5.628	5.781	5.678	0.101	5.826	0.117	5.969	0.122
	70-phyllite	60	2747	5.695	5.806	5.931						
	97-metagabbro	5	2920	6.018	6.526	6.828						
	98-metagabbro	5	2847	6.282	6.558	6.685						
	total	100										
Coldfoot	71-schist (quartz-mica schist)	10	2765	6.001	6.226	6.375	5.580	0.201	5.808	0.154	5.988	0.098
	93-quartz-mica schist	10	2708	5.845	6.054	6.147						
	80-schist (calc-schist)	60	2657	5.393	5.666	5.910						
	quartz schist*	20		5.8	5.9	5.95						
	total	100										
Hammond	72-marble (Skajit)	5	2691	6.314	6.463	6.575	5.738	0.183	5.915	0.153	6.055	0.150
	79-marble (Skajit)	5	2654	6.063	6.370	6.592						
	78-slate (Beaucoup)	25	2756	5.742	5.859	5.988						
	calc-schist*	25		5.4	5.65	5.8						
	73-phyllite (meta-volcaniclastic-silicic)	40	2739	5.835	5.991	6.125						
	total	100										
Endicott Mountains												
South of Toyuk thrust fault	75-phyllite (Hunt Fork)	90	2736	5.785	5.840	5.905	5.788	0.010	5.850	0.016	5.916	0.019
	77-quartzite (Noatuk)	4	2808	5.980	6.137	6.252						
	74-conglomerate (Kanayut)	0.5	2664	5.793	5.874	5.957						
	sandstone*	5		5.7	5.8	5.85						
	shale*	0.5		5.75	5.85	5.9						
	total	100										
North of Toyuk thrust fault	shale (Hunt Fork)*	2		5.75	5.85	5.9	5.564	0.106	5.764	0.161	5.901	0.220
	sandstone (Noatak)*	2		5.95	6.0	6.05						
	76-conglomerate (Kanayut)	12	2609	5.446	5.653	5.821						
	sandstone (Kanayut)*	24		5.45	5.6	5.7						
	shale (Kanayut)*	24		5.5	5.7	5.8						
	shale (Kayak and Etivluk)*	10		5.75	5.8	5.85						
	88-limestone (Lisburne Group)	26	2621	5.669	5.987	6.223						
	total	100										
North Slope												
Franklinian rocks	83-phyllite (Doonerak window)	75	2684	5.789	5.865	5.950	5.952	0.225	6.029	0.225	6.115	0.225
	84-greenstone (Doonerak window)	20	2943	6.577	6.653	6.736						
	quartzite, carbonate*	5		5.9	6.0	6.1						
	total	100										
Ellesmerian rocks	89-argillite (Echooka)	5	3069	6.024	6.125	6.239	5.861	0.055	5.998	0.014	6.123	0.023
	82-arg. limest. (Lisb. Grp; Doonerak window)	40	2656	5.786	5.980	6.141						
	shale, siltstone, minor carbonate/ sandstone*	55		5.9	6.0	6.1						
	total	100										
Brookian rocks	90-siltstone (Fortress Mountain)	50	2642	5.162	5.303	5.460	5.112	0.051	5.301	0.002	5.482	0.022
	91-siltstone (Nanushuk Group)	50	2661	5.061	5.298	5.503						
	total	100										

Laboratory measurements of density and velocity for suite of rock types in each terrane or subterrane of Brooks Range and vicinity are given. Velocity measurements are tabulated for pressures of 50, 100, and 200 MPa. Rock percentages in each terrane or subterrane along transect are estimated, and weighted average of laboratory rock velocity is calculated.

†Includes sample number and formation name, where available.

*Rock velocities were inferred in order to calculate weighted average.

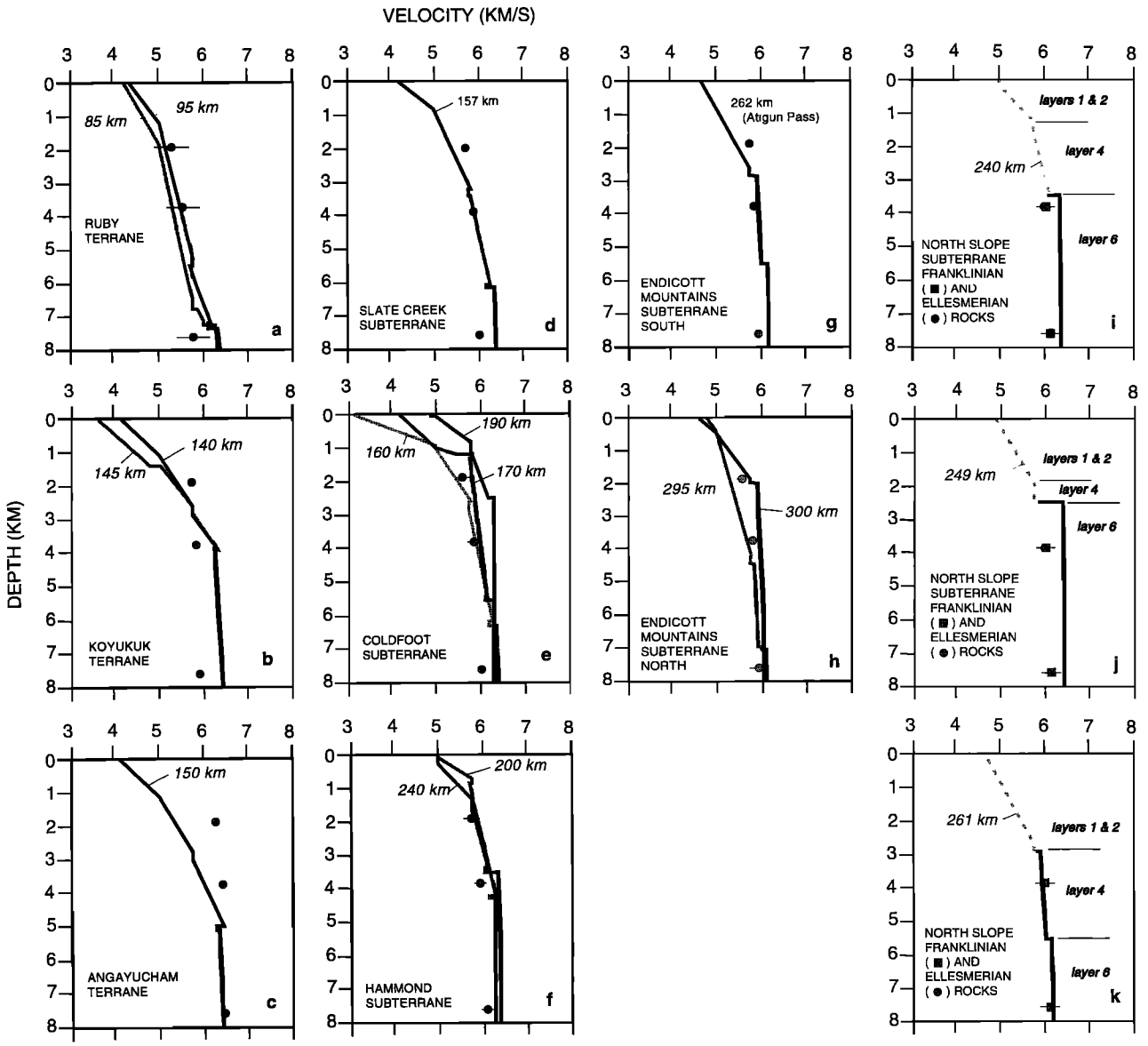

Figure 5. Velocity-depth curves for the terranes and subterranes of the Brooks Range and vicinity. Numbers in kilometers identify the model coordinate for each curve (see Plate 2). Dots with error bars are average laboratory velocities for each terrane or subterrane at 50, 100, and 200 MPa (see Table 2). Layer numbers are identified in Figures 5i–5k. Note that in Figures 5a–5k, average velocities of North Slope Franklinian and Ellesmerian rocks, as calculated, are indistinguishable (the symbols are superimposed); however, the addition of more greenstone to the average of Franklinian rocks (sample 84, Table 2) would move this average higher.

270 and 310 km. North of this interval, it shoals, reaching about 44 km depth at about model coordinate 380 km. The shoaling is well constrained by precritical reflections from shot points on the North Slope. In the image of *Wissinger et al.* [this issue], vertical incidence reflections in zone F2 dip uniformly northward from the Moho at about model coordinate 250 to a depth of about 62 km at model coordinate 330 km, where the image of these reflections is lost. There is no indication of dip reversal or northward shoaling of these reflections to correlate with the wide-angle image. Thus the vertical incidence and wide-angle images of the sub-Moho reflective zone are not fully consistent in the region 270–330 km. Further work is warranted.

North Slope

Cenozoic through Franklinian rocks are penetrated in the northernmost wells on the North Slope (e.g., Kadler no. 1 well, Plate 2 and Figure 1). This section can be followed southward with regularity in other wells to model coordinate 425 km and can be projected farther southward into the region controlled by seismic data, beginning near model coordinate 400 km. Brookian rocks are characterized in the model interval 425–500 km by a strong positive velocity gradient in their upper part, with velocities reaching as much as 4.0 km/s, and a weak or negative velocity gradient in their lower part (Figure 1).

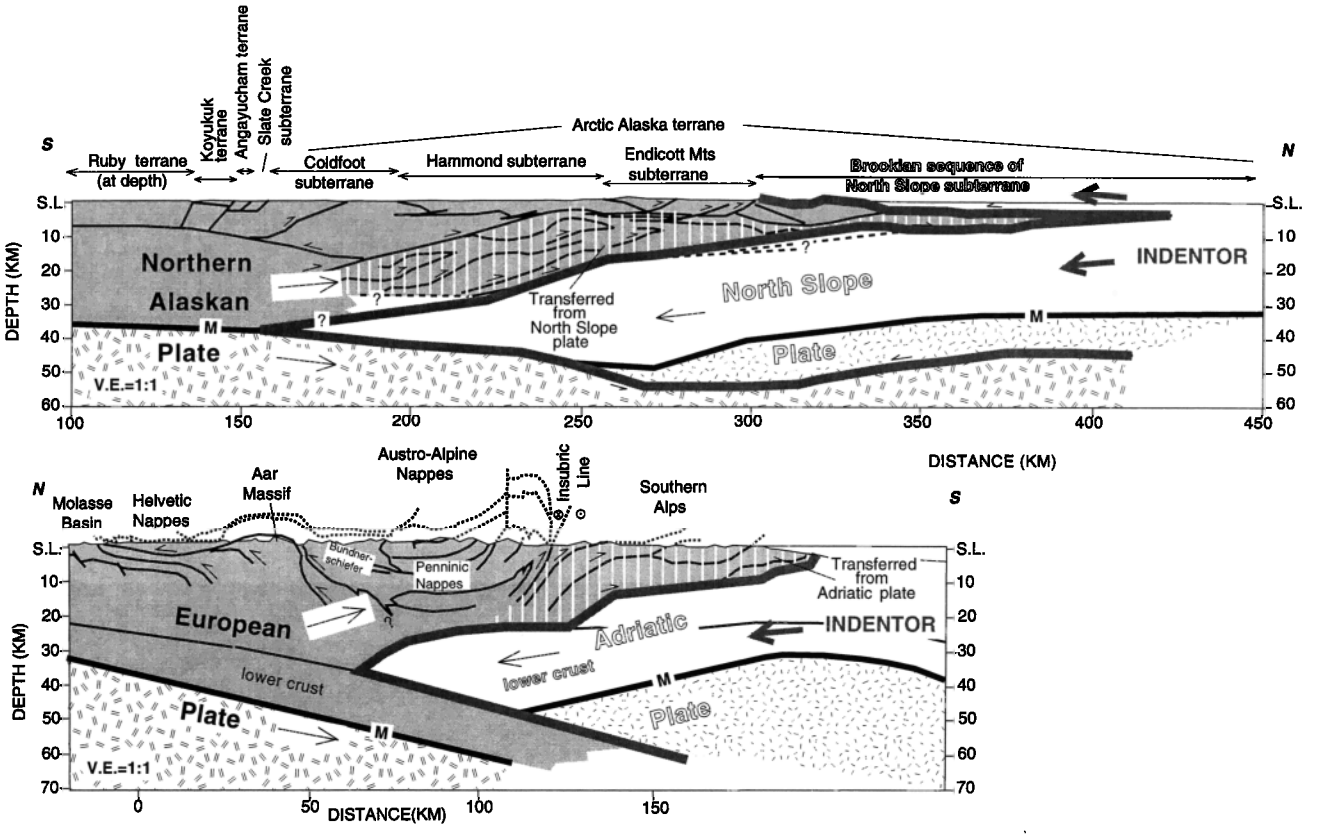

Figure 6. Comparison of cross sections of Brooks Range and European Alps. Cross section of Alps modified from *Ye et al.* [1995] and *Schmid et al.* [1996]. Crust is gray (indented plate) or blank (indentor plate); mantle has double-tick pattern (indented plate) or single-tick pattern (indentor plate). Heavy gray line separates indented plates (northern Alaskan and European plates) from indentor plates (North Slope and Adriatic plates). Rock that has been clearly transferred from indentor plate to indented plate is indicated with vertical white lines.

Below the Lower Cretaceous unconformity (LCU), uppermost Ellesmerian rocks (Kingak Shale) have velocities of 4.0 km/s or less and also have a weak or negative velocity gradient. Permo-Triassic Ellesmerian rocks in the oil wells represent a positive velocity step to as much as 4.5 km/s, and carbonate rocks of the Lisburne Group represent a velocity step to as much as 5.7 km/s. On the basis of comparison of model, oil well, and laboratory velocities between model coordinates 350 and 400 km, layers 1 and 2 are interpreted as Brookian rocks; layers 4 and 5, as chiefly Permo-Triassic Ellesmerian rocks; and layer 6, as carbonate rocks of the Lisburne Group (Plate 3). This interpretation is undoubtedly overly simplified.

Triplication of the Lisburne Group is required in the north limb of the synformal structure between model coordinates 320 and 340 km (Plate 3). At least three clear reflections can be seen here (N5, N6, N7, Figures 2e and 2f); velocity of the upper layer is constrained by refractions to be about 5.6 km/s; velocity of the deeper layers is poorly constrained but consistent with a velocity range of 5.7–6.2 km/s. Interpreted rocks in the south limb of the antiformal structure (model coordinates 300–320 km) were discussed above under "Endicott Mountains subterrane." Rocks overlying the antiformal structure (velocity ~5.0 km/s) are interpreted as post-Lisburne Group Ellesmerian rocks and rocks of the Delong Mountains subterrane. A small outcrop of the latter, presumably a window, is located at model coordinate 323 km [*Mull et al.*, this issue].

Thrust faulting extends as far northward as the Susie no. 1 well (model coordinate 420 km, Plate 2) but cannot be seen in the next well to the north, although broad warping is seen in the nearby Franklin Bluffs [e.g., *Grantz et al.*, 1991]. Moderate deformation, including folds and thrust faults, begins southward of model coordinate 400. The Lupine no. 1 well, for example, penetrates an anticline in Brookian rocks. Accordingly, we have shown the Atigun Gorge thrust fault (a backthrust) extending northward as far as model coordinate 420 km, where it is joined by the interpreted basal decollement. Another branch of a backthrust is added between model coordinates 350 and 380 km to account for interpreted thickening of post-Lisburne Group Ellesmerian rocks, but this branch is semischematic.

Discussion

The cross section (Plate 3) was drawn as simply as possible, using model velocities and wide-angle reflections as guides for deep structure and inferences from outcrops and wells for shallow structure. Further refinement may be possible when the cross section is balanced, but balancing is beyond the scope of this paper. Balancing, of course, assumes movement of rock bodies strictly in the plane of the cross section. This assumption may be good for much of the Brooks Range but may fail near the northern range front, where some geologic contacts

strike obliquely to the profile (see Plate 1), and also in the southern Brooks Range where strike-slip displacement is interpreted to have occurred on the Malamute and Kobuk-South Fork faults, along the south front of the Brooks Range.

At the northern range front the deformational style seen in Lisburne Group rocks of the EMS and NSS where they are structurally juxtaposed is a stacking of limestone horses [*Wallace et al.*, this issue] (see also *Oldow et al.* [1987] and *Cole et al.* [this issue] for examples of this structural style farther west). This style differs from the "detachment folding" deformational style documented in the northeastern Brooks Range by *Wallace and Hanks* [1990], in which carbonate rocks of the Lisburne Group and overlying rocks are folded tightly in anticlinoria and synclinoria above a detachment fault in the Kayak Shale. The northward change from imbrication to detachment folding in Lisburne Group rocks is exposed east of the transect at about the latitude of SP142 (model coordinate 315, Plate 3).

The opposing vergence represented by zones B/D and zone E is reminiscent of opposing vergence observed and modeled in many orogenic belts [e.g., *Beaumont and Quinlan*, 1994]. The Moho depression beneath the transect, however, is located to one side rather than beneath the region of convergence of zones B/D and zone E and thus differs from most other orogenic belts. This geometry may be explained by (1) thrusting of a deformable plate onto a less deformable plate or (2) a complex history of orogeny that cannot be modeled as a single collisional event. In interpretation 1, represented by Plate 3, the plate on the south, here called the Northern Alaskan plate, splits in the lower crust or at the Moho, with the middle and upper crust, or all of the crust, overriding the interpreted tectonic wedge and the mantle underthrusting the wedge [cf. *Beaumont and Quinlan*, 1994, model 1]. The wedge, here called the North Slope plate, is stiffer than the Northern Alaskan plate and has undergone downwarping as it is loaded by the upper part of the Northern Alaskan plate. The parallelism of the basal decollement north of 220 km, the Moho north of 275 km, and the sub-Moho reflector north of 320 km, is suggestive of a downwarped plate. In addition to downwarping, however, large masses of rock have been transferred from the North Slope plate to the Northern Alaskan plate (Plate 3 and Figure 6).

In interpretation 2, a tectonic history that includes Late Jurassic-Early Cretaceous shortening, mid-Cretaceous extension, and renewed Cretaceous-Cenozoic shortening, with differing loci of maximum deformation, may have created the crustal root where it exists at present; the sub-Moho reflector is unexplained in this interpretation.

The European Alps is another orogenic belt where one plate is interpreted to be split by another plate into two parts, with the lower part underthrusting and the upper part duplexing above the "indentor" plate (Figure 6) [e.g., *Ye et al.*, 1995; *Schmid et al.*, 1996]. In the Alps the European plate is split by the Adriatic plate, and both the European lower crust and mantle are interpreted to underthrust the Adriatic plate. The interpretation that European lower crust is being underthrust is permitted because of an observed gap between the European and Adriatic Moho's. In contrast, no such Moho gap can be observed in the Brooks Range orogen; the Moho's of the Northern Alaskan and North Slope plates appear to be continuous with one another. Another difference between the Alps and northern Alaska is that most surface geologic structures in these two orogens verge oppositely. It is interesting that in both the Alps and northern Alaska the smaller continental fragment (North Slope and Adriatic), which rifted from a larger continental body (Canadian Arctic margin and Africa), became the indentor.

Conclusion

This study has concentrated on extending prior seismic imaging studies of the Brooks Range northward onto the North Slope and downward into the mantle. In the tectonic interpretation of the final image of this study (Plate 3), the Northern Alaskan plate is split in the lower crust or at the Moho in the southern Brooks Range by a relatively more rigid indentor plate, or tectonic wedge, that consists of the crust of the North Slope and a 10- to 15-km-thick layer of mantle. The middle and upper crust of the Northern Alaskan plate, or all of the crust, is uplifted and deformed by duplexing above the indentor, and the mantle of this plate underthrusts the indentor. Thus mantle of two different origins (and different seismic velocities) is juxtaposed, giving rise to a prominent sub-Moho reflector.

Acknowledgments. This experiment was funded in part by U.S. Geological Survey Deep Continental Studies Program and by the National Science Foundation Geophysics Program (grants EAR 8905222 and EAR 9105002 and IRIS subagreements 0127 and 0140). Our field crew in Alaska included, in addition to the authors, 33 people without whose hard work and courage under adverse field conditions, this beautiful data set could never have been collected. We have listed these people in the paper by *Murphy et al.* [1993]. We would like to reiterate special thanks to Ed Criley, supervisor of U.S. Geological Survey field operations; Isa Asudeh, supervisor of Canadian Geological Survey field operations; and Jim Fowler, manager of the IRIS/PASSCAL program. In addition, persons from seven government and private agencies assisted us with the difficult jobs of permitting and providing logistical support. We have also listed these people in the paper by *Murphy et al.* [1993]. Finally, we thank Bruce Beaudoin, Tom Brocher, Doug Christensen, William Hinze, George Plafker, and Walter Mooney for helpful reviews of earlier versions of this manuscript and Jorg Ansorge, Chris Beaumont, Nihal Okaya, and Wes Wallace for discussions that influenced our interpretation. Financial support for the laboratory velocity measurements was provided by the Office of Naval Research and the National Science Foundation Continental Dynamics Program.

References

Beaumont, C., and G. Quinlan, A geodynamic framework for interpreting crustal-scale seismic-reflectivity patterns in compressional orogens, *Geophys. J. Int.*, *116*, 754–783, 1994.

Blundell, D. J., The Zurich I model, how the interpretation fared, in *Workshop Proceedings: Interpretations of Seismic Wave Propagation in Laterally Heterogeneous Structures*, edited by D. M. Finlayson and J. Ansorge, *Rep. 258*, pp. 177–179, Bur. of Miner. Resour., Geol., and Geophys., Canberra, Australia, 1984.

Christensen, N. I., Measurements of dynamic properties of rock at elevated pressures and temperatures, in *Measurements of Rock Properties at Elevated Pressures and Temperatures*, edited by H. J. Pincus and E. R. Hoskins, pp. 93–107, Am. Soc. for Testing and Mater., Philadelphia, Pa., 1995.

Cole, F., K. J. Bird, J. Toro, F. Roure, P. B. O'Sullivan, M. Pawlewicz, and D. G. Howell, An integrated model for the tectonic development of the Northern Brooks Range and Coleville Basin, 250 km west of the Trans-Alaska crustal transect, *J. Geophys. Res.*, this issue.

Fuis, G. S., W. J. Lutter, A. R. Levander, and E. S. Wissinger, Wide-angle reflections help clarify interpretation of the CMP image of the Brooks Range, Arctic Alaska (abstract), *Eos Trans. AGU*, *73*, 371, 1992.

Fuis, G. S., W. J. Lutter, A. R. Levander, E. S. Wissinger, T. E. Moore, and N. I. Christensen, Seismic images of the Brooks Range, Arctic Alaska, reveal crustal-scale duplexing, *Geology*, *23*, 65–68, 1995.

Gottschalk, R. R., and J. S. Oldow, Low-angle normal faults in the

south-central Brooks Range fold and thrust belt, Alaska, *Geology*, *16*, 395–399, 1988.

Grantz, A., and S. D. May, Rifting history and structural development of the continental margin north of Alaska, in *Studies in Continental Margin Geology*, edited by J. S. Watkins and C. L. Drake, *AAPG Mem.*, *34*, 77–100, 1983.

Grantz, A., T. E. Moore, and S. Roeske, Gulf of Alaska to Arctic Ocean, *Centen. Cont. Ocean Transect 15*, 72 pp., 3 sheets, scale 1:500,000, Geol. Soc. of Am., Boulder, Colo., 1991.

Gryc, G. (Ed.), Geology and exploration of the National Petroleum Reserve in Alaska, 1974 to 1982, *U.S. Geol. Surv. Prof. Pap.*, *1399*, 940 pp., 1988.

Levander, A., G. S. Fuis, E. S. Wissinger, W. J. Lutter, J. S. Oldow, and T. E. Moore, Seismic images of the Brooks Range fold and thrust belt, Arctic Alaska, from an integrated seismic reflection/refraction experiment, *Tectonophysics*, *232*, 13–30, 1994.

Luetgert, J. H., MacRay—Interactive two-dimensional seismic raytracing for the Macintosh, *U.S. Geol. Surv. Open File Rep.*, *92-356*, 43 pp., 1992.

Mayfield, C. F., I. L. Tailleur, and I. Ellersieck, Stratigraphy, structure, and palinspastic synthesis of the western Brooks Range, northwestern Alaska, *U.S. Geological Survey Open File Rep.*, *83-779*, 58 pp., 5 plates, 1983.

Meissner, R., *The Continental Crust: A Geophysical Approach*, 426 pp., Academic, San Diego, Calif., 1986.

Miller, E. L., and T. L. Hudson, Mid-Cretaceous extensional fragmentation of a Jurassic-Early Cretaceous compressional orogen, Alaska, *Tectonics*, *10*, 781–796, 1991.

Mooney, W. D., Seismic methods for determining earthquake source parameters and lithospheric structure, in *Geophysical Framework of the Continental United States*, edited by L. Pakiser and W. D. Mooney, *Mem. Geol. Soc. Am.*, *172*, 11–34, 1989.

Moore, T. E., W. K. Wallace, K. J. Bird, S. M. Karl, C. G. Mull, and J. T. Dillon, Geology of northern Alaska, in *The Geology of North America*, vol. G-1, *The Geology of Alaska*, edited by G. Plafker and H. C. Berg, pp. 49–140, Geol. Soc. of Am., Boulder, Colo., 1994.

Moore, T. E., W. K. Wallace, C. G. Mull, K. E. Adams, G. Plafker, and W. J. Nokleberg, Crustal implications of bedrock geology along the Trans-Alaska Crustal Transect (TACT) in the Brooks Range, northern Alaska, *J. Geophys. Res.*, this issue.

Mull, C. G., D. H. Roeder, I. L. Tailleur, G. H. Pessel, A. Grantz, and S. D. May, Brooks Range and Arctic slope to Beaufort Sea, Alaska, scale 1:500,000, *Geol. Soc. Am. Map Chart Ser.*, *MC-28S*, 1987.

Mull, C. G., R. A. Glenn, and K. E. Adams, Tectonic evolution of the central Brooks Range Mountain front: Evidence from the Atigun Gorge region, *J. Geophys. Res.*, this issue.

Murphy, J. M., G. S. Fuis, A. R. Levander, W. J. Lutter, E. E. Criley, S. A. Henrys, I. Asudeh, and J. C. Fowler, Data report for the 1990 seismic reflection/refraction experiment in the Brooks Range, Arctic Alaska, *U.S. Geol. Surv. Open File Rep.*, *93-265*, 128 pp., 1993.

Oldow, J. S., C. M. Seidensticker, J. C. Phelps, F. E. Julian, R. R. Gottschalk, K. W. Boler, J. W. Handschy, and H. G. Avé Lallement, Balanced cross sections through the central Brooks Range, and North Slope, Arctic Alaska, 19 pp., 8 sheets, scales 1:500,000 and 1:66,666, Am. Assoc. of Pet. Geol., Tulsa, Okla., 1987.

Oldow, J. S., A. W. Bally, H. G. Avé Lallement, and W. P. Leeman, Phanerozoic evolution of the North American Cordillera, in *The Geology of North America*, vol. A, *The Geology of North America: An Overview*, edited by A. W. Bally and A. R. Palmer, pp. 139–232, Geol. Soc. of Am., 1989.

O'Sullivan, P. B., P. F. Green, S. C. Bergman, J. Decker, I. R. Duddy, A. J. W. Gleadow, and D. L. Turner, Multiple phases of Tertiary uplift and erosion in the Arctic National Wildlife Refuge, Alaska, revealed by apatite fission track analysis, *AAPG Bull.*, *77*, 359–385, 1993.

O'Sullivan, P. B., T. E. Moore, and J. M. Murphy, Tertiary uplift of the Mt. Doonerak antiform, central Brooks Range, Alaska: Apatite fission track evidence from the Trans-Alaska Crustal Transect, in *Central Brooks Range*, edited by J. S. Oldow and H. G. Ave Lallement, *Mem. Geol. Soc. Am.*, in press, 1997.

Plafker, G., and H. C. Berg, Overview of the geology and tectonic evolution of Alaska, in *The Geology of North America*, vol. G-1, *The Geology of Alaska*, edited by G. Plafker and H. C. Berg, pp. 989–1021, Geol. Soc. of Am., Boulder, Colo., 1994.

Roeder, D., and C. G. Mull, Tectonics of Brooks Range ophiolites, Alaska, *AAPG Bull.*, *62*, 1696–1702, 1978.

Schmid, S. M., O. A. Pfiffner, N. Froitzheim, G. Schoenborn, and E. Kissling, Geophysical-geological transect and tectonic evolution of the Swiss-Italian Alps, *Tectonics*, *15*, 1036–1064, 1996.

Wahrhaftig, C., Physiographic divisions of Alaska, *U.S. Geol. Surv. Prof. Pap.*, *482*, 52 pp., 1965.

Wallace, W. K., and C. L. Hanks, Structural provinces of the northeastern Brooks Range, Arctic National Wildlife Refuge, Alaska, *AAPG Bull.*, *74*, 1100–1118, 1990.

Wallace, W. K., T. E. Moore, and G. Plafker, Multistory duplexes with forward dipping roofs, north central Brooks Range, Alaska, *J. Geophys. Res.*, this issue.

Wissinger, E. S., A. Levander, and N. I. Christensen, Seismic images of crustal duplexing and continental subduction in the Brooks Range, *J. Geophys. Res.*, this issue.

Ye, S., J. Ansorge, E. Kissling, and St. Mueller, Crustal structure beneath the eastern Swiss Alps derived from seismic refraction data, *Tectonophysics*, *242*, 199–221, 1995.

K. J. Bird, G. S. Fuis, T. E. Moore, and J. M. Murphy, U.S. Geological Survey, 345 Middlefield Road, MS 977, Menlo Park, CA 94025. (e-mail: kbird@octopus.wr.usgs.gov; fuis@andreas.wr.usgs.gov; tmoore@mojave.wr.usgs.gov; murphy@andreas.wr.usgs.gov)

N. I. Christensen, Department of Geosciences, Purdue University, West Lafayette, IN 49707. (e-mail: chris@geo.purdue.edu)

W. J. Lutter, Department of Geology and Geophysics, University of Wisconsin at Madison, Madison, WI 53706-1692. (e-mail: wlutter@geology.wisc.edu)

(Received June 14, 1996; revised December 9, 1996;
accepted December 19, 1996.)